Harnessing the power of anti-amyloidogenic polyglutamine binding peptide 1: A computational and biophysical approach to antimicrobial prediction

Francisco Ramos-Martín, François Peltier, Saoussen Oueslati, Liam Cousin, Mariam Rima, Marie Perret, Laurie Bibens, Emmanuel Sevin, Viviane Antonietti, Sophie Da Nascimento, et al.

International Journal of Biological Macromolecules 318 (2025) 144938

Contents lists available at ScienceDirect

International Journal of Biological Macromolecules

journal homepage: www.elsevier.com/locate/ijbiomac

Harnessing the power of anti-amyloidogenic polyglutamine binding peptide 1: A computational and biophysical approach to antimicrobial prediction

Francisco Ramos-Martín [a,*], François Peltier [b], Saoussen Oueslati [c], Liam Cousin [d], Mariam Rima [c], Marie Perret [b], Laurie Bibens [b], Emmanuel Sevin [d], Viviane Antonietti [b], Sophie Da Nascimento [b], Catherine Sarazin [a], Fabien Gosselet [d], Thierry Naas [c], Pascal Sonnet [b], Nicola D'Amelio [a,*]

[a] Unité de Génie Enzymatique et Cellulaire, UMR 7025 CNRS, Université de Picardie Jules Verne, Amiens 80039, France
[b] Agents Infectieux, Résistance et Chimiothérapie, AGIR UR 4294, Université de Picardie Jules Verne, UFR de Pharmacie, Amiens 80037, France
[c] Université Paris Sud Faculté de Médecine Hôpital de Bicêtre Service de Bactériologie Bâtiment Broca, 3ème étage, 78 rue du Gal Leclerc, Paris 94270, France
[d] Laboratoire de la Barrière Hémato-Encéphalique (LBHE), UR 2465, Université de Artois, F-62300 Lens, France

ARTICLE INFO

Keywords:
Antimicrobial peptide
Neurodegeneration
Anti-amyloidogenesis

ABSTRACT

In this work, we demonstrate for the first time the antimicrobial activity of poly-Q binding peptide 1 (QBP1), an anti-amyloidogenic molecule previously identified by phage display for its ability to bind and inhibit the aggregation of polyglutamine proteins like Huntingtin, but also α-synuclein and prion models. Intriguingly, sequence analysis by the ADAPTABLE web server highlighted QBP1's potential antifungal and antibacterial activity, which we have now confirmed experimentally. A theoretical basis for the predicted mechanism of action was provided by molecular dynamics simulations revealing the role of QBP1 aggregates promoting membrane disruption and specific interactions between QBP1 and bacterial and fungal phospholipids, further substantiated by solid-state NMR studies. Using primary human cells, we demonstrated that QBP1 does not display toxicity at high concentrations. Finally, our data demonstrate QBP1's efficacy against some strains of *Bacillus cereus*, *B. mojavensis*, *Staphylococcus aureus*, *S. epidermidis*, *Micrococcus luteus*, *Enterococcus faecalis*, *Escherichia coli*, and *Candida*. This unexpected dual function of QBP1 opens new avenues for therapeutic development, potentially restoring the putative antimicrobial protection exerted by many amyloidogenic proteins.

1. Introduction

Intrinsically disordered proteins have attracted significant attention in the last few decades due to their link with neurodegenerative disorders. These proteins display a complex equilibrium of conformers in solution [1–3]; some are able to aggregate and form toxic oligomers, eventually leading to the formation of amyloids. It is now widely accepted that amyloid fibrils are generally non-toxic, while oligomeric intermediates are often associated with toxicity [4,5]. Amyloids are noncovalent oligomers of extended β-sheets that self-assemble laterally, forming twisted fibers or fibrils of around 10 nm in diameter. Although they have been linked to neurodegeneration, they also play functional roles in biological processes across different species [2,6], including amyloids linked to memory consolidation (CPEB/Orb2) [7,8].

To date, around 40 peptides and proteins have been found to form amyloid deposits linked to human disorders such as amyloid-beta peptide involved in the development of the senile plaques associated with Alzheimer's disease (AD), α-synuclein involved in Parkinson's disease (PD), microtubule-associated protein tau involved in AD and some dementias, prion protein involved in Creutzfeldt-Jakob disease [9], islet amyloid polypeptide (IAPP) involved in type II diabetes, pulmonary surfactant-associated protein C in pulmonary alveolar proteinosis, and poly-Q expansion diseases like Huntington's disease (HD), among others [2,10,11].

Interestingly, amyloidogenic proteins share similarities with host defense peptides (HDPs) [12], an important class of rather unstructured molecules with antimicrobial activity also called antimicrobial peptides (AMPs) [13–16]. They exert their antimicrobial action by destabilizing the membrane of the pathogen, targeting exposed phospholipids. Although they generally form alpha-helical structures upon binding to

* Corresponding author.
E-mail addresses: francisco.ramos@u-picardie.fr (F. Ramos-Martín), nicola.damelio@u-picardie.fr (N. D'Amelio).

https://doi.org/10.1016/j.ijbiomac.2025.144938
Received 25 November 2024; Received in revised form 26 May 2025; Accepted 2 June 2025
Available online 3 June 2025

their targets, a model has been suggested describing amyloid formation by some HDPs [13]. Monomers of these peptides adopt an α-helical structure at the membrane interface, which leads to membrane insertion and self-assembly. Subsequently, these species would undergo conformational changes to form β-sheet multimers that could further aggregate, generating the β-structures associated with amyloid fibrils [13]. It seems that a relevant number of HDPs are able to adopt this structure to exert their antimicrobial action [13,14,17–19].

Indeed, many amyloidogenic proteins can also act as HDPs. For example, it has been reported that Aβ40 and Aβ42 peptides may act as amyloidogenic HDPs [12,19–21] and their neurotoxicity could be related to the aberrant use of their amyloid-mediated antimicrobial mechanisms [14,21,22]. This raises the intriguing hypothesis that neurodegeneration could originate from previous viral, bacterial, or fungal infections [21,23–34]. Indeed, some studies have suggested that PD onset could sometimes be caused by the germination of spores produced by bacteria or fungi [35], such as *Malassezia*, *Botrytis*, *Candida*, or *Fusarium* [36,37]. Similarly to Aβ40 and Aβ42 peptides, antimicrobial activity has been described for the microtubule binding sites on tau protein [38], the N-terminal segment of the prion protein [39,40], and IAPP [12,14,22,41,42]. While Aβ and IAPP have shown activity against *Streptococcus pneumoniae*, α-synuclein can attack *Escherichia coli*, *Pseudomonas aeruginosa*, *Staphylococcus epidermidis*, and *Staphylococcus aureus* and displays antifungal activity against *Aspergillus flavus*, *Aspergillus fumigatus*, *Candida albicans*, *Candida tropicalis*, and *Rhizoctonia solani* [28,43–45]. Furthermore, aggregation-prone surfactant protein C plays a role in immunity targeting bacteria, viruses, or fungi [10,46,47].

Due to the antimicrobial action of proteins and peptides involved in neurodegeneration, strategies focused on their suppression might increase the rate of infections. For example, in PD patients treated with molecules affecting α-synuclein aggregation, an increase in fungal infection was observed [23–28,31,36,48,49]. Likewise, in vivo experiments have demonstrated an increase in the protection against pathogens in models overexpressing these toxic proteins [50–52].

PolyQ Binding Peptide 1 (QBP1) was isolated from a phage-display screening designed to find peptides capable of blocking polyQ aggregation [53], implicated in several neurological pathologies like HD or spinocerebellar ataxia [54]. Its optimization led to the final sequence Ac-Trp-Lys-Trp-Trp-Pro-Gly-Ile-Phe-NH_2 [55]. It adopts a preferential conformation in solution stabilized by a hydrophobic cluster [56] and successfully blocks polyQ-induced neurodegeneration in *Drosophila melanogaster* and mice [53,57–59], while its scrambled versions are ineffective and unstructured [56].

Not only does QBP1 inhibit polyQ amyloidogenesis, but it is also effective with a variety of amyloidogenic proteins, including the A53T mutant of α-synuclein, Sup35NM prion [1], and TDP-43 (involved in amyotrophic lateral sclerosis) [60]. Interestingly, due to the role of some amyloids in memory, QBP1 has been studied as a way to prevent memory consolidation, which could be desired in certain situations [7,8,61]. QBP1 has also been used in combination with other peptides to obtain an anti-amyloidogenic synergistic action [62], and different strategies have been developed to improve its passage through the blood-brain barrier (BBB) [63–65], some involving the conjugation of cell-penetrating peptides (CPPs) [66].

While the antimicrobial activity of QBP1 has never been reported to date, sequence alignment with the web server ADAPTABLE [67] highlights strong similarities with several AMPs, suggesting a beneficial antibacterial and antifungal activity of this anti-amyloidogenic drug. In this work, we discover by biophysical methods a direct interaction with bacterial and fungal membrane lipids and by microbiology assays a remarkable activity against *Bacillus cereus*, *B. mojavensis*, *Staphylococcus aureus*, *S. epidermidis*, *Micrococcus luteus*, *Enterococcus faecalis*, *Escherichia coli*, and *Candida*. The molecular mechanisms at the atomic level are elucidated by means of solid-state NMR spectroscopy and molecular dynamics (MD) simulations, showing the important role of lysine in position 2 (K2) in the process of bacterial and fungal membrane destabilization.

The confirmation of QBP1 as an AMP would help to partially restore the putative antimicrobial activity of some amyloidogenic proteins. Additionally, some AMPs have already been used with success as labeled markers for those infections [21,68–70]. Current efforts for efficient delivery through the Blood-brain barrier (BBB) could help in the fight against several pathogens that can either infect the brain after surgeries [71] or pass the barrier to cause brain infections, especially in patients affected by neurodegenerative diseases such as *S. aureus*, *Candida albicans*, *Chlamydia pneumoniae*, Herpes simplex, West Nile virus, *E. coli*, and *Cryptococcus neoformans* [72–79].

2. Results and discussion

2.1. Sequence-property alignment suggests antibacterial and antifungal activities of QBP1

To get insight into the antimicrobial properties of QBP1, we analyzed its sequence by means of the ADAPTABLE web server [67]. The peptide was used as bait and compared with the full ADAPTABLE database to generate a sequence-related family whose members are in the order of sequence similarity (Fig. 1). Within the same family, 90 % of the members exhibit antibacterial (*S. aureus, P. aeruginosa,* or *Enterococcus* sp., among others) but also antifungal and antiviral activities.

The best-representing peptide [67] of the QBP1 family found by ADAPTABLE is Indolicidin (6–13) [80], an AMP active against both gram-negative and gram-positive bacteria. Drawbacks in the use of Indolicidin as an antibacterial include moderate hemolytic activity [80] and damage to lymphocytes T [81]. Its structural optimization has led to a core structure with a good compromise between antibacterial and hemolytic activities [80,82]. MD simulations have supported these investigations in the attempt to understand the main factors driving its affinity for different types of membranes [83,84], showing the strengths of this technique for the tuning of AMP activities [85]. In addition to its antimicrobial activity, Indolicidin has been suggested to be antiviral (against HIV and Herpes simplex virus [80,86,87]), antifungal [88] and antiparasitic (against *Giardia lamblia* protozoa [89]).

2.2. The interaction of QBP1 with biomimetic membranes by MD simulations

To understand the molecular basis of a possible antimicrobial activity of QBP1, we performed MD simulations in the presence of different kinds of lipid bilayers mimicking the composition of different cell membranes (Fig. 2).

2.2.1. Interaction and toxicity towards mammalian cells

2.2.1.1. Interaction with biomimetic membranes. Phosphatidylcholine (PC) is the predominant phospholipid in the outer leaflets of mammalian cell membranes while being virtually absent in bacterial membranes [89]. To investigate the interaction between QBP1 and membrane systems of increasing complexity (Fig. 2A-C), we initiated our study with a simplified model of a pure POPC bilayer (Fig. 2A). Subsequently, we enriched this model with cholesterol (CHOL, Fig. 2B) and sphingomyelin (SM, Fig. 2C).

In the pure POPC system, a salt bridge forms between the amine group of K2 and the phosphate oxygen atoms of the membrane (Fig. S1). This interaction facilitates the insertion of the W1 side chain into the bilayer (Fig. S2). While this interaction is relatively superficial, it nonetheless disrupts the membrane order, as evidenced by a decrease in the order parameter of phospholipid acyl chains (Fig. S3). By quantifying the degree of molecular order on a scale of 0 to 1 [91], the order parameter provides a quantitative measure of lipid dynamics, which in turn could be linked to membrane destabilization induced by molecular

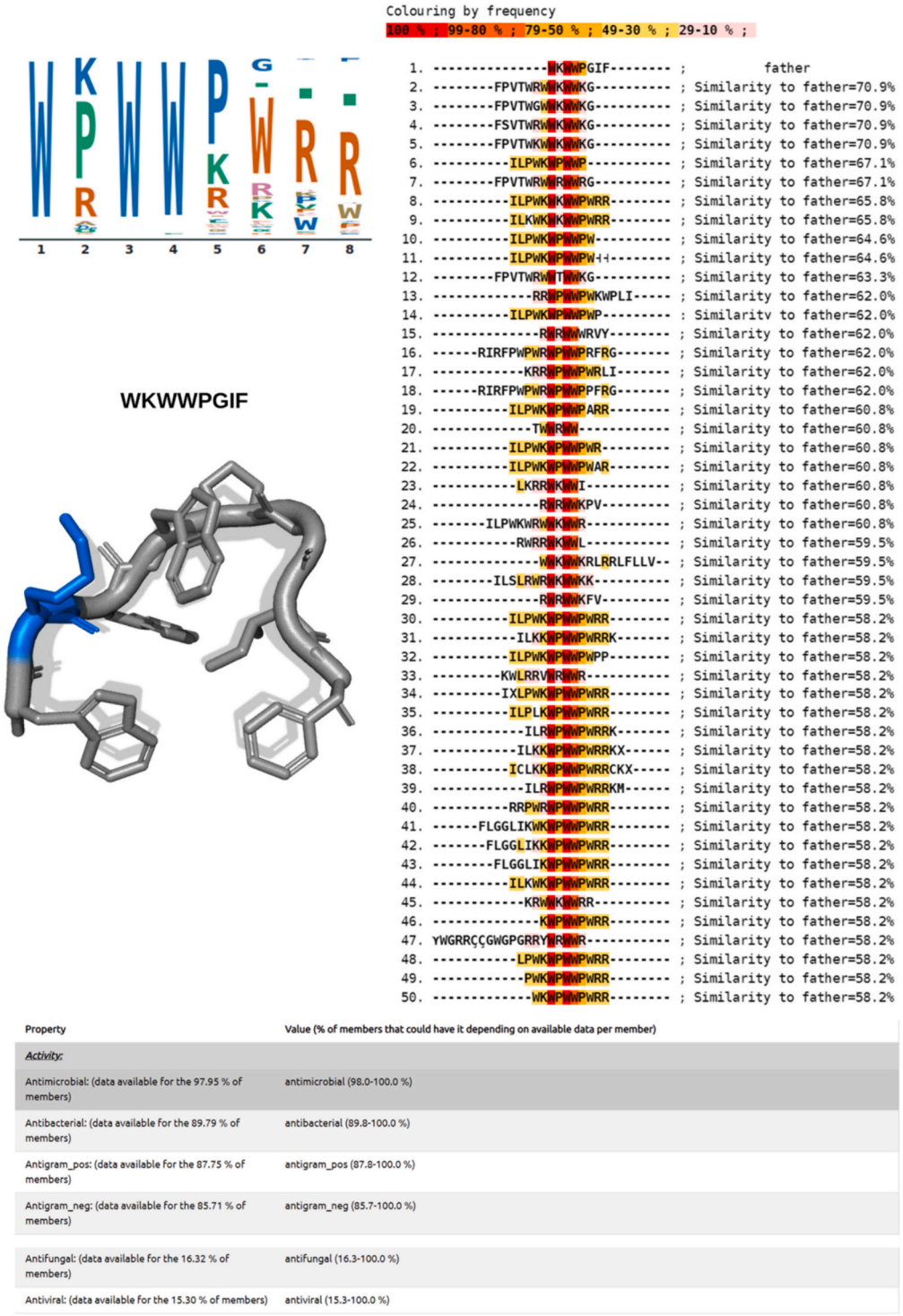

Property	Value (% of members that could have it depending on available data per member)
Activity:	
Antimicrobial: (data available for the 97.95 % of members)	antimicrobial (98.0-100.0 %)
Antibacterial: (data available for the 89.79 % of members)	antibacterial (89.8-100.0 %)
Antigram_pos: (data available for the 87.75 % of members)	antigram_pos (87.8-100.0 %)
Antigram_neg: (data available for the 85.71 % of members)	antigram_neg (85.7-100.0 %)
Antifungal: (data available for the 16.32 % of members)	antifungal (16.3-100.0 %)
Antiviral: (data available for the 15.30 % of members)	antiviral (15.3-100.0 %)

Fig. 1. First 50 members of the family created by sequence alignment of QBP1 with the entries of the ADAPTABLE database. A summary of the activities of the members is given at the bottom. The NMR structure of QBP1 (BMRB entry 25022) [56,90] is shown as a "tube" where side chains are represented as sticks. Color code: positively charged residues in light blue, hydrophobic or small chain residues in light gray.

interactions. Analyzing the order parameter for each C—H bond of the acyl chain allows us to assess the impact of QBP1 on the membrane's inner core, even in the case of superficial interactions.

While QBP1 appears to perturb pure POPC bilayers, this interaction is significantly diminished in more complex membrane models. The presence of cholesterol substantially reduces the formation of the salt bridge and hinders the insertion of W1 side chains (Figs. S4, S5). The bulky trimethylated choline headgroup introduces substantial steric hindrance and the zwitterionic nature of the lipid offers little electrostatic incentive for interaction with the positively charged peptide. To further improve our model, we incorporated sphingomyelin, a key component of mammalian membranes, particularly abundant in the brain [92,93]. In this more complex model (POPC 35 %, SM 35 %, CHOL 30 %), the interaction observed with pure POPC bilayers is almost entirely abolished (Figs. S4, S5), and the order parameter remains largely unaffected (Fig. S3).

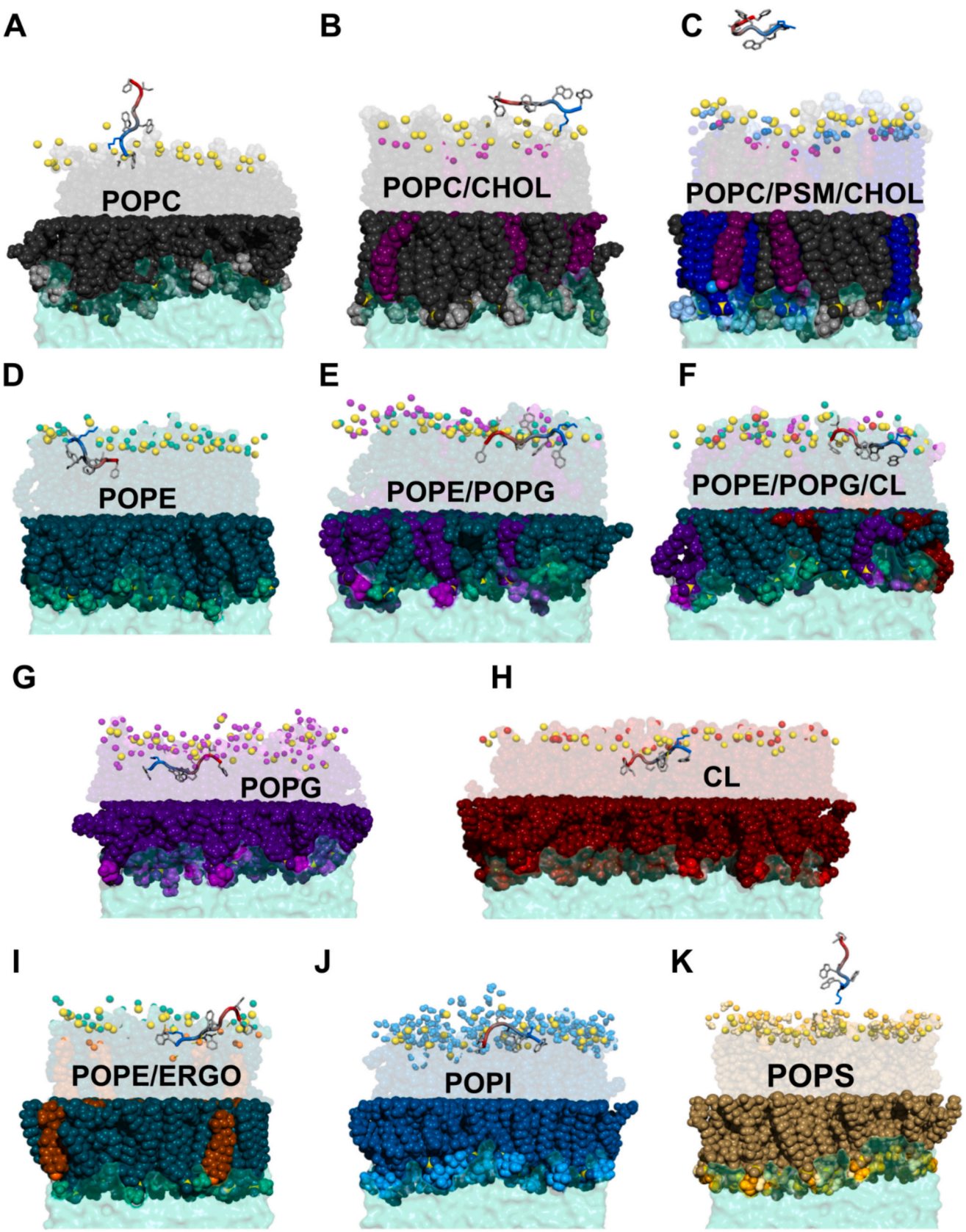

(caption on next page)

Fig. 2. Representative MD snapshots of Ac-QBP1-NH_2 interacting with several membranes of variable phospholipid compositions. (A) 1-palmitoyl-2-oleoyl-glycero-3-phosphocholine (POPC); (B) POPC/cholesterol (CHOL); (C) POPC/Palmitoyl sphingomyelin (SM)/CHO; (D) 1-palmitoyl-2-oleoyl-sn-glycero-3-phosphoethanolamine (POPE); (E) POPE/1-palmitoyl-2-oleoyl-sn-glycero-3-phospho-(1′-rac-glycerol) (POPG); (F) POPE/POPG/cardiolipin (CL); (G) POPG; (H) CL; (I) POPE/ergosterol (ERGO); (J) 1-palmitoyl-2-oleoyl-sn-glycero-3-phosphoinositol (POPI); (K) 1-palmitoyl-2-oleoyl-sn-glycero-3-phosphatidylserine (POPS). Color code: phosphorus atom: yellow; POPC black (body) and light gray (choline group); POPS brown (body), gold (headgroup), light yellow (amine of the headgroup) and orange (carboxyl of the headgroup); POPE dark green (body), turquoise (headgroup), light green (amine of the headgroup); POPG dark violet (body), violet (headgroup), light violet (hydroxyls of the headgroup); POPI blue (body), light blue (headgroup), cyan (hydroxyls of the headgroup); PSM deep blue (body), baby blue (choline), cobalt blue (amide nitrogen), cerulean blue (non-phosphate oxygen atoms); CL dark red (body) and light red (headgroup); ERGO dark orange (body) and light orange (hydroxyl); CHOL purple (body) and light purple (hydroxyl). For clarity, only functional groups of headgroups are shown (spheres) in the upper leaflet. Ac-QBP1-NH_2 peptide is shown as a "tube" colored from blue (N-terminus) to red (C-terminus). Side chains are shown as sticks with the following color code: positively charged (blue), negatively charged (red), nonpolar (light gray), and polar (yellow). PSM refers to SM.

The full insertion of a peptide into a biological membrane is a relatively slow process when simulated using all-atom molecular dynamics (MD). To capture such long-timescale events, advanced sampling techniques like metadynamics, coarse-grained simulations, steered MD, umbrella sampling, replica exchange, or others [85] are often employed. Alternatively, the free energy barriers to peptide insertion can be bypassed by initiating the simulation with an internalized peptide. For this reason, we repeated all simulations with QBP1 positioned within the membrane core. Despite these significantly different starting conditions, the simulations consistently reproduced the behavior observed in the previous calculations: after an initial rapid interaction with the POPC surface, QBP1 subsequently dissociated from both POPC/CHO and POPC/CHO/SM bilayers while exhibiting only weak, superficial interactions with pure POPC. These findings align with the extensive in vivo testing of QBP1, which has not shown a remarkable toxicity [7,53,57,58,61–63].

2.2.1.2. Toxicity towards human primary cells mimicking the blood-brain barrier. Experiments shown above demonstrate that QBP1 poorly interacts with mammalian biomimetic membranes, thus strongly suggesting that there is no toxicity towards mammalian cells. In order to experimentally verify this hypothesis, we have tested QBP1 toxicity at 2 concentrations (5 and 50 μM) using a human model of the blood-brain barrier (BBB). BBB isolates the brain from xenobiotics found in the peripheral circulation and protects neurons from harmful molecules. This model is based on the co-cultivation of human primary endothelial cells with human brain pericytes during 6 days. After this period, the endothelial cells acquire the phenotype of the human BBB, in particular the tight junction (TJ) structures that closely interact with the membranes to strongly seal the endothelial cells together. Among the proteins forming these TJs, we focused on Zonula Occludens 1 and Claudin-5.

This model is routinely used in order to assess molecule toxicity on the central nervous system [94–97]. Toxicity is assessed by measuring the diffusion of a small fluorescent marker, the sodium fluorescein (NaFlu), across the endothelial cell monolayer to calculate a permeability coefficient (Pe). As shown in Fig. 3A, the Pe of LY is not modified in QBP1-treated cell conditions (5 and 50 μM) when compared to the untreated condition. On the contrary, when cells are treated with 3 % DMSO, which is our positive control of BBB breakdown and cell toxicity, we observe a significant increase in the Pe NaFlu. Fig. 3B shows that only DMSO treatment alters CLAUDIN-5 and ZO-1 localization at the cell membranes and then disrupts the BBB. QBP1 treatments do not affect the TJ.

2.2.2. The interaction with bacterial phospholipids

The outer leaflet of gram-positive and gram-negative bacterial membranes contains high amounts of the zwitterionic phosphatidylethanolamine (PE) [98] and is enriched in anionic phospholipids such as phosphatidylglycerol (PG) and cardiolipin (CL). PE and PG can create a rich network of interactions [99,100] and their ratio can be used by bacteria to modulate the permeability and stability of their membranes [98].

To study the effect of QBP1 on bacterial membranes, we investigated its interaction with POPE/POPG and POPE/POPG/CL bilayers but also their pure components (Fig. 2D-H), whose analysis can highlight lipid-specific interactions.

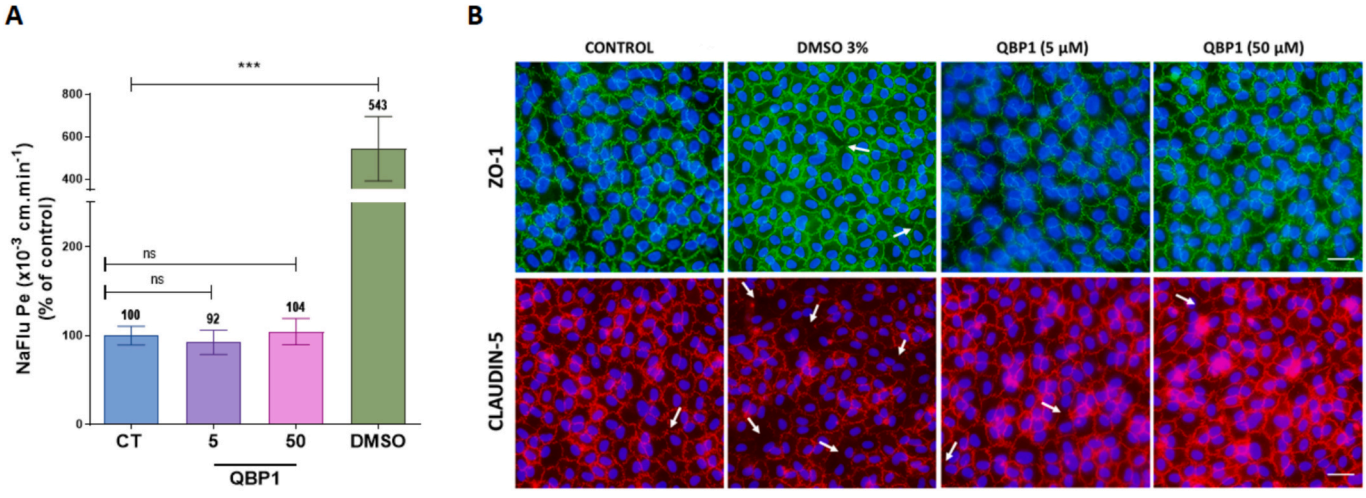

Fig. 3. QBP1 does not display any toxicity on human cells. (A) QBP1 was added during 24 h at 5 or 50 μM to the luminal compartment of the human BBB model, and the paracellular permeability coefficient (Pe) of the fluorescent marker sodium fluorescein (NaFlu) was measured as indicated in the Experimental Section. 3 % DMSO was used as a positive control of BBB disruption. Data were analyzed using GraphPad Prism® software version 8.0 (Dotmatics, Boston, MA, USA). A one-way ANOVA test was performed, and the values are expressed as the mean ± standard deviation (SD). The thresholds for statistical significance were set as $p < 0.05$ (*), $p < 0.01$ (**), and $p < 0.001$ (***) compared with the control (or untreated) conditions (n = 9–1; ns = not significant). (B) ZO-1 and CLDN-5, two key player proteins forming the tight junctions sealing BBB endothelial cells together, were studied by immunofluorescence. White arrows show disruption of the TJ proteins localization at the cell membrane. Scale Bar = 2.5 μm.

2.2.2.1. The interaction with POPE bilayers. PE is one of the main lipids present in the outer leaflets of many bacteria, parasites, and fungi and can be found exposed on the surface of cancer cells [98]. In our simulations, QBP1 promptly associates with POPE bilayers by means of a salt bridge between the side chain of K2 and the PE phosphate oxygen atoms (see polar contacts in Fig. S1 and a significant MD snapshot in Fig. 2D). Unlike pure POPC, the peptide is fully internalized, establishing van der Waals interactions with the entire sequence within the membrane interior (see apolar contacts in Fig. S2). Notably, the peptide approaches the membrane via its C-terminus, likely to mitigate electrostatic repulsion between the lysine side chain and the positive charge of PE amine groups. Once internalized, the peptide aligns parallel to the membrane surface, positioning itself beneath the plane defined by PE phosphate groups. This orientation facilitates occasional hydrogen bonding with PE by means of backbone polar atoms, particularly the amide of G6 (Fig. S1). These results are reproduced when the simulation is started by initially placing QBP1 at the center of the bilayer, supporting our findings (Fig. S6).

The interaction with PE fluidifies the membrane as described by the lower-order parameters of the palmitoyl chains (Fig. S3). The perturbation can also be monitored by the analysis of electron density profiles, in which the position of the phospholipid head group is indicated by the peripheral maxima and the very center of the bilayer is described by the central minimum. In particular, we observe an increase in the central minimum generally ascribed to lipid interdigitation [101] (Fig. S7).

2.2.2.2. The interaction with POPG and CL bilayers. PG is a phospholipid characteristic of prokaryotes and not common in eukaryotes, being only present at certain organs and locations [98]. It is a key component of many bacterial membranes. Cardiolipin (CL) is a phospholipid structurally related to PG, present in mitochondria but also in bacteria. Investigating QBP1's interactions with PG and CL bilayers provides valuable insights into its potential antibacterial activity.

As in the case of POPE bilayers, QBP1 strongly interacts with POPG bilayers (Fig. 2G). The larger size of the PG headgroup makes the penetration of QBP1 more challenging, but the peptide promptly inserts perpendicularly and subsequently lies parallel to the membrane surface under the plane described by PG phosphate groups (an orientation also obtained when the peptide is initially placed inside the bilayer). The same polar contacts observed in the case of POPE bilayers are also established in POPG bilayers, the most important being the salt bridge between the side chain of K2 and the PG phosphate oxygen atoms (Figs. S1, S6). Also in this case, extensive van der Waals interactions are established all along the QBP1 sequence (Fig. S2). The deep insertion of QBP1 leads to membrane fluidification (Fig. S3), and electron density profiles reveal lipid interdigitation, albeit less pronounced than with POPE bilayers (Fig. S7).

When simulating QBP1 in CL bilayers (Fig. 2H), we observed a highly similar interaction pattern, with comparable polar and apolar contacts (Figs. S8, S9). The increased frequency of interactions with CL acyl chains likely stems from their greater accessibility. These findings were consistent, even when QBP1 was initially placed within the bilayer center (Fig. S10).

2.2.2.3. Complex bacterial mixtures. Simulations of QBP1 in pure POPE, POPG, and CL lipid bilayers revealed highly similar structural and interaction profiles. Notably, the peptide exhibited deep insertion (Fig. S9) and formed stable salt bridges between K2 and the phosphate oxygen atoms of all lipid types (Fig. S8). When examining more complex bacterial membrane models, such as PE/PG (Fig. 2E) and PE/PG/CL (Fig. 2F) bilayers, we observed consistent results. In both cases, QBP1 displayed deep insertion and salt bridge formation. Interestingly, while polar contacts in POPE/POPG mixtures were evenly distributed between PE and PG, a clear preference for CL was evident in POPE/POPG/CL models, likely due to the larger accessibility of the CL's negative charges (CL's phosphate groups are less buried than those of PG) attracting the positively charged QBP1 (Figs. S8).

To assess binding affinity, we calculated ΔG_{bind} for Ac-QBP1-NH_2 in various lipid environments. Molecular Mechanics with Generalized-Born Surface Area (MM-GBSA) has become one of the most popular methods to estimate binding free energies. This method achieves a good balance between accuracy and computational efficiency and is less computationally demanding than alchemical free energy methods [102]. While generally positive values, indicative of unfavorable binding, were observed for PC-containing mixtures, significantly stronger binding (negative ΔG_{bind}) was found for bacterial and fungal phospholipids (PE, PG, PI, CL) (Table S1). QBP1 exhibited a marked affinity for bacterial membrane models and their individual components. Rapid penetration into the bilayer (Fig. S9) led to significant disruption of the lipid organization, as evidenced by altered order parameter values (Fig. S3). These results indicate that QBP1 could indeed have antibacterial activity, killing the target microbe by destabilizing their membranes, a common mechanism used by HDPs.

2.2.3. The interaction with the fungal membrane

Infections caused by fungi such as *Malassezia*, *Botrytis*, *Candida*, or *Fusarium* have been proposed as causative agents of neurodegenerative disorders, and they can also constitute a serious issue in elderly and immunosuppressed patients [35–37]. Fungal membranes are rich in PC and PE phospholipids but also ergosterol (ERGO), which is the main sterol in fungal organisms and a common target for antifungal compounds [98]. Other common phospholipids found in the outer leaflet of fungal membranes are phosphatidylinositol (PI) and phosphatidylserine (PS), mostly located in the inner leaflet of mammalian cells [98]. For these reasons, we investigated the interaction of QBP1 with ERGO, PS, and PI (Fig. 2I-K).

2.2.3.1. The interaction of QBP1 with ergosterol. In our simulations with bilayers containing 70 % of POPE and 30 % of ergosterol, we observe a very important interaction between QBP1 polar atoms and the hydroxyl of ergosterol (Figs. S4 and 2I). As we showed for POPE models, QBP1 tends to dispose parallel to the membrane surface, lying in a plane just beneath that described by phospholipid phosphate groups. This is due to the salt bridge anchoring QBP1 to phosphate oxygen atoms by means of the side chain of K2. In this location, the hydroxyl of ergosterol is promptly available for the formation of H-bonds with QBP1 polar atoms. Not only are backbone amide N and O atoms involved, but also the N_ε nitrogen of tryptophan residues. Furthermore, QBP1's aromatic side chains engage in direct van der Waals interactions with ergosterol (Fig. S5). These polar and apolar interactions enable QBP1 to exert sufficient force to displace ergosterol molecules to the opposite leaflet, creating additional space for itself (Fig. S11). This behavior was consistently observed across multiple simulation runs, even when QBP1 was initially positioned within the membrane interior.

The substantial alteration of membrane lipid organization is evident in the significant changes in both the order parameter (Fig. S3) and the area per lipid (Fig. S12). The latter parameter is a useful indicator of membrane invagination observed in the presence of QBP1, characterized by an increase in the area per lipid in the distal leaflet and a corresponding decrease in the proximal leaflet. Overall, these findings support an antifungal activity of QBP1.

2.2.3.2. The interaction of QBP1 with POPI and POPS bilayers. As previously mentioned, PS and PI are often found in fungal membranes. The interest in PS stems from the fact that microbial infections (but also cancer) can cause its exposure on mammal cells in a process known as apoptotic mimicry [98].

When studying the interaction of QBP1 with POPI bilayers (Fig. 2J), we observe a complete penetration of the peptide, leading to fluidification of the membrane (Fig. S3). The inserted peptide establishes the

usual sets of polar and apolar contacts described in POPE bilayers (Figs. S8, S9): a salt bridge with the side chain of K2 and van der Waals interactions with the entire sequence.

In the case of POPS bilayers (Fig. 2K), the dense network of interactions between the amino and carboxylate moieties of the lipid head groups creates a sterically hindered membrane surface. This reduced accessibility limits the ability of QBP1 to penetrate the bilayer. While occasional salt bridge formation between the K2 side chain amino group and PS carboxylates can occur (Fig. S1), these interactions are not sufficient to drive significant peptide insertion.

Interestingly, when simulations are initiated with QBP1 already positioned within the bilayer, the peptide remains trapped, unable to escape. This suggests that the apparent poor penetration observed in simulations where the peptide is initially added to the exterior of the bilayer may be a consequence of insufficient simulation time to capture the rare event of successful membrane insertion.

2.3. QBP1 aggregates enhance bacterial membrane disruption by exhibiting increased affinity for negatively charged membranes

QBP1 contains one hydrophilic residue in an 8-long sequence, protected termini, and 4 aromatic residues prone to stacking phenomena. Such a hydrophobic sequence might well have a tendency to aggregate in water solution at high concentrations. This is why we repeated our simulations in the presence of 8 peptides.

Indeed, significant peptide aggregation was observed in all simulations, as evidenced by the contact map in Fig. S13. These multimeric structures lack a well-defined conformation. Despite the aggregation, the fluidifying effect of QBP1 on target membranes is amplified, as indicated by the increased order parameter perturbations (Fig. 4). Furthermore, electron density profiles (Fig. S14) show more pronounced alterations, and area-per-lipid measurements reveal substantial membrane invaginations (Fig. S15). Instead of competing with peptide penetration, aggregation on top of the membrane could actually favor membrane instability and penetration of QBP1, as in the case of simulation with multiple peptides interacting with PS (Fig. S16). Simulations suggest that the aggregation of QBP1, driven by the stacking of its aromatic residues, plays a key role in overcoming this limitation. By forming multimers, QBP1 enhances its effective positive charge, boosting its electrostatic interaction with anionic membranes while remaining far from neutral ones (Fig. 5). This aggregation serves two critical functions: first, it prevents individual peptides from inserting into neutral membranes composed of phosphatidylcholine and cholesterol, and second, it facilitates the preferential targeting of negatively charged bacterial membranes by concentrating positive charges locally. Once the aggregate approaches the membrane surface, our simulations reveal that individual QBP1 peptides can penetrate the bilayer independently, disrupting its internal organization as evidenced by a reduction in the order parameter within the membrane core.

2.4. The importance of the protection of QBP1 termini

QBP1 is often studied acetylated at the N-terminus and amidated at its C-terminus (Ac-QBP1-NH_2). Our simulations suggest that the addition of charged termini to the unprotected peptide can significantly impact its behavior. The N-terminal amine and C-terminal carboxylate groups enable additional salt bridge formation with lipid head groups, enhancing peptide-membrane interactions, leading to potential increased activity.

In simulations with mammalian (POPC and POPC/CHOL, Figs. S17A, B) and bacterial (POPE, POPG, CL, and their mixtures, Figs. S17C-G) lipids, the unprotected peptide exhibits frequent salt bridge interactions compared to its protected counterpart (compare Figs. S18, S19, and S22 with Figs. S1, S4, and S8). These salt bridges lead to membrane disruption (Fig. S24) and peptide penetration (Figs. S20, S21, S23), in which the C-terminal carboxylate group often remains exposed to the membrane exterior.

In contrast, in simulations with fungal-like lipids (ergosterol, POPI, and PS), similar considerations hold, but the strong interaction between the unprotected peptide and phospholipid head groups can hinder the peptide's ability to interact with ergosterol, a key component of fungal membranes (compare Fig. S19 with Fig. S4). With PS and PI, the interaction appears superficial (Figs. S17I, J) but stronger than in protected QBP1 because the peptide grabs the phosphate oxygen atoms by means of its two amino groups (N-terminus and lysine side chain) (compare Figs. S18 and S6 for PS and Figs. S22 and S8 for PI). The strength of such interaction prevents further internalization, at least in the time window examined and blocks the penetration of unprotected QBP1, especially in POPS bilayers (Fig. S20).

Despite these differences, both the protected and unprotected peptides induce significant membrane perturbations, as evidenced by changes in order parameters (Figs. S3 and S24) and electron density profiles (Figs. S7 and S25). However, the reduced selectivity of the unprotected peptide, which appears to interact also with mammalian membrane models, may introduce potential toxicity.

2.5. Studies by solid-state NMR spectroscopy confirm the tropism of QBP1 for bacterial-like lipids

Multilamellar vesicles (MLVs), or liposomes, provide a fairly realistic model of biological membranes suitable for NMR spectroscopy [103]. We have used them to study the effect of QBP1 on model membranes mimicking mammalian membranes (PC, PC/CHOL, and PC/CHOL/SM), bacterial membranes (containing PE, PG, and CL), and fungal membranes (PE, PS, and PI).

Deuterium NMR (^{2}H NMR) spectroscopy of deuterated phospholipid acyl chains provides insights into membrane dynamics. The magnitude of the quadrupolar splitting observed for each deuterium atom scales with its mobility, due to the averaging of the C—D bond orientations with respect to the external magnetic field [91,103]. Highly mobile deuteriums, such as those in methyl groups, experience minimal splitting and appear near the spectrum's center. In contrast, deuteriums in rigid regions, including the plateau region (carbons 2–6) near the ester bond, exhibit larger splittings and appear at the spectrum's edges.

Deuterium NMR spectra of palmitoyl-chain-deuterated membranes (Fig. 6) reveal significant fluidification in bacterial and fungal models (i.e., containing PE, PG, PS, and CL lipids), particularly those composed of PE/PG and PE/PG/CL mixtures, which closely mimic the composition of several bacteria [98]. The incorporation of peptides into these membranes leads to a systematic decrease in T_2. We attribute this to a chemical exchange mechanism between lipids directly interacting with the peptide and those in the surrounding bilayer. The rapid lateral diffusion of lipids within the vesicle facilitates this exchange, leading to an averaging of local environments and a measurable reduction in T_2 with a consequent increase of linewidth and an apparent signal loss.

POPC models, mimicking mammalian membranes, also show some fluidification (Fig. 6A), which might suggest potential toxicity. However, the addition of cholesterol significantly mitigates this effect (Fig. 6G). Interestingly, some degree of fluidification is observed in PC/eggSM/CHOL models (Fig. 6H), which seems to contradict MD simulation results and several in vivo studies [53,57–59]. This discrepancy might be attributed to the difference in chain length between eggSM and POPC, potentially influencing liposome packing and membrane dynamics [104].

2.6. Microbiological activity tests

In order to ascertain our hypothesis on the antimicrobial activity of QBP1, we measured the minimal inhibitory concentration (MIC) towards some fungi, gram-negative, and gram-positive bacteria (Tables 1 and S2).

Curiously, the activity is highly dependent on the media used

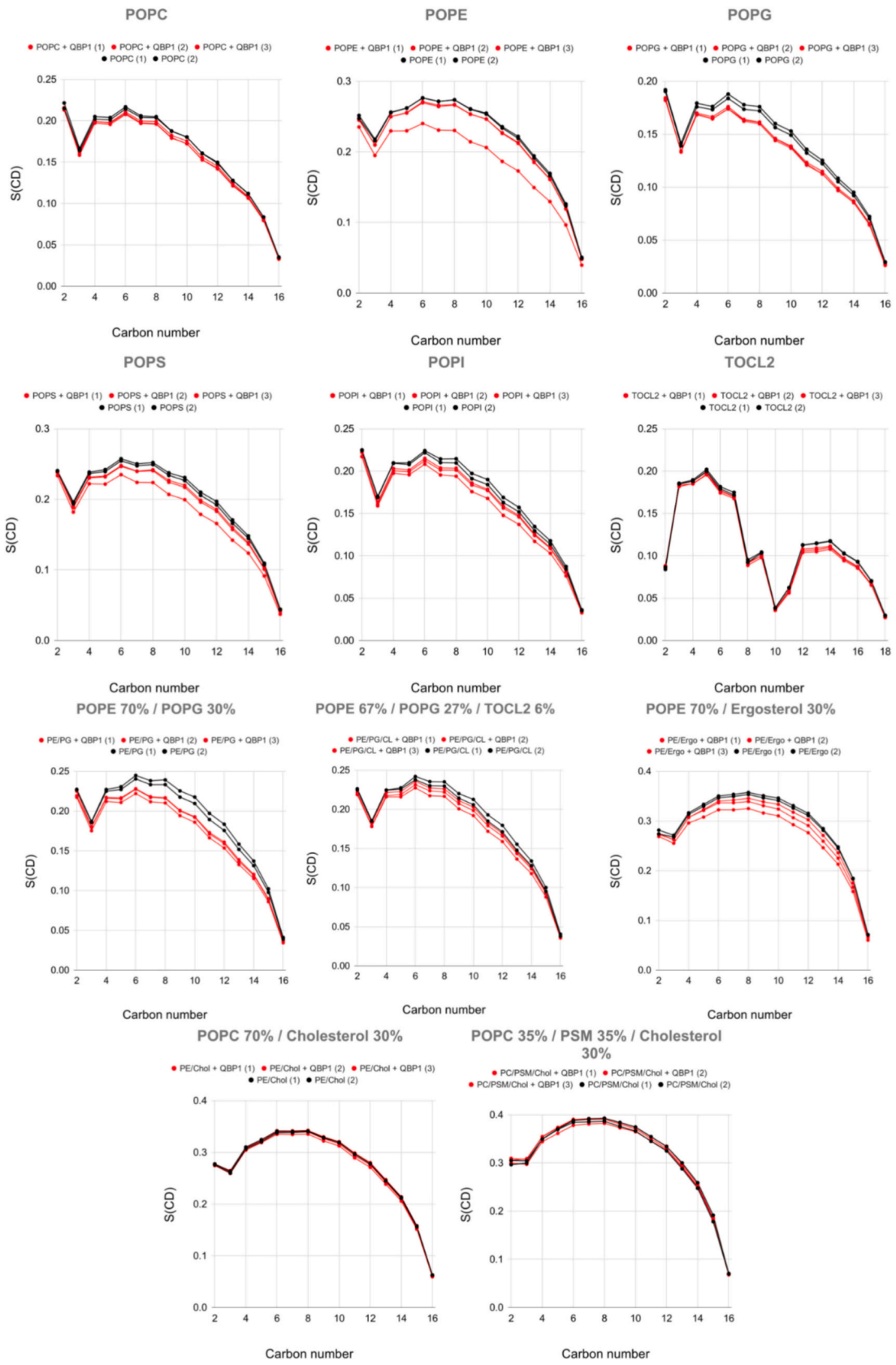

Fig. 4. Order parameter of C—H moieties of palmitoyl side chains in membranes containing various phospholipid compositions as calculated from multiple repetitions of MD simulations in the absence (2 repetitions in black labeled as 1 and 2) and in the presence (3 repetitions in red labeled from 1 to 3) of eight Ac-QBP1-NH_2 peptides.

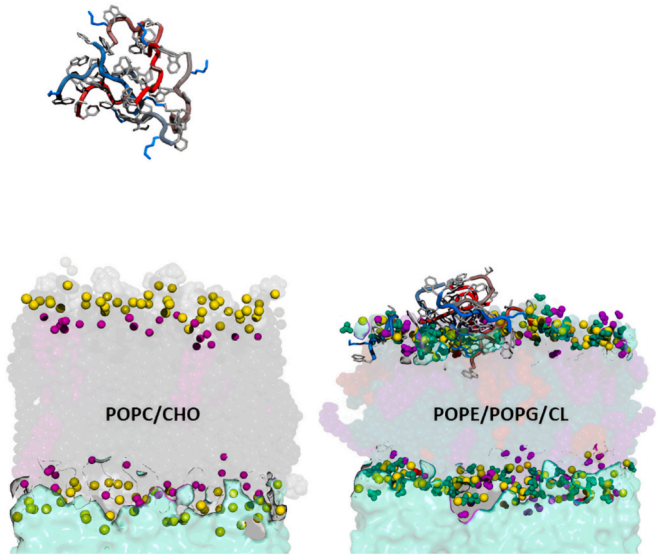

Fig. 5. Representative MD snapshots of Ac-QBP1-NH_2 interacting with several membranes of variable phospholipid compositions. (left) 1-palmitoyl-2-oleoyl-glycero-3-phosphocholine POPC/CHOL; (right) POPE/POPG/CL. Color code as in Fig. 2.

(Table S2). As previously reported [105–107], the presence of Ca^{2+} and Mg^{2+} ions can impair the antimicrobial activities of many AMPs. This is why we also did the measurements using non-cation-adjusted MHB media (MHB). As predicted by our simulations, deprotection of termini results in more potent activity (compare MIC values for QBP1-NH_2 with Ac-QBP1-NH_2, Table S2), probably due to the instauration of more salt bridges between phospholipids and the positively charged N-terminal amino group.

We decided then to test more microorganism species and strains using the non-acetylated QBP1 version and MHB medium, finding values as low as 4 and 8 mg/L against *Micrococcus luteus*, *Bacillus mojavensis*, and one strain of *Candida* (Table 1). In other cases, the activity is moderate (e.g., *E. coli*, *Enterococcus faecalis*, *B. cereus*, *M. luteus*, *S. aureus*, and *S. epidermidis*) but in line with many other antimicrobial peptides and natural compounds (Tables 1 and S2) [108–114].

QBP1 exhibits significant activity against Gram-positive bacteria and certain *Candida* strains but shows limited effectiveness against Gram-negative species. Gram-negative bacteria possess an outer membrane rich in lipopolysaccharides (which vary among species), creating a barrier that restricts access to the inner membrane. This protective layer is further reinforced by resistance mechanisms such as efflux pumps and proteases [115]. In contrast, Gram-positive bacteria and fungi lack this outer membrane. Although they have thick cell walls—composed of peptidoglycan in bacteria and glucans/mannans in fungi—these structures do not appear to hinder QBP1 from reaching its target.

The susceptibility of *Candida* strains varies significantly, with some showing low minimum inhibitory concentrations (MICs; 4–32 mg/L) and others exhibiting high resistance (>256 mg/L). This variability can be attributed to differences in membrane composition and functionality [116]. Key factors include ergosterol content (a critical fungal membrane component), cell wall thickness (affecting permeability), and the presence of efflux pumps or proteases that degrade antimicrobial peptides. Among Gram-positive bacteria, MIC variability may arise from differences in cell wall structure, membrane composition, surface charge density, and the presence of efflux systems or proteases.

These data pave the way for the future improvement of this antimicrobial activity without impairing its anti-amyloidogenic one.

3. Conclusions

In this work, we have first predicted and verified the antibacterial and antifungal activities of the anti-amyloidogenic peptide QBP1. Such activities were predicted by sequence alignment and supported by solid-state NMR spectroscopy and MD simulations with a variety of biomimetic membranes (Fig. 7).

Simulations provided a detailed description of QBP1's possible mechanism of action at the atomic level. In particular, we have found that QBP1 does not damage complex models of the external leaflet of mammalian cells containing PC, cholesterol, and sphingomyelin. Neither toxicity is detected with our human BBB model, in agreement with the lack of toxicity reported in previous in vivo studies. On the contrary, QBP1 was found to interact extensively and penetrate not only bacterial and fungal membranes but also the membranes of their pure components (PE, PG, CL, PS, and PI). A common feature is the establishment of a salt bridge between the side chain of K2 and the phosphate oxygen atoms, anchoring QBP1 to phosphate groups once the peptide is internalized. The formation of numerous van der Waals contacts between the apolar side chains of QBP1 and the acyl chains of phospholipid stabilizes the interaction. Inside its target membranes, QBP1 does not assume an ordered structure but lies in a plane parallel to the surface underneath the phosphate moieties. This location destabilizes membrane ordering, especially in the presence of ergosterol, whose hydroxyl is readily available for H-bonding.

The observed antimicrobial activity aligns with previous research demonstrating the efficient membrane penetration of tryptophan-rich peptides, particularly in gram-positive bacteria [117,118] and in cases where these residues are optimally placed in the sequence [119,120]. QBP1, with its three tryptophan residues, leverages this property. Indeed, tryptophan was shown to play a key role in the cellular uptake of cell-penetrating peptides (CPPs) [118,121], due to the favorable free energy of the insertion of its aromatic side chain into the plasma membrane [121–123]. In the case of QBP1, our simulation shows that the presence of tryptophan triggers the formation of aggregates with high positive charge. These aggregates may serve a dual function: first, by recruiting monomers, they limit the insertion of individual peptides into neutral membranes composed of phosphatidylcholine and cholesterol; second, by accumulating positive charges, they increase the affinity for negatively charged bacterial membranes.

While increasing the number of tryptophan residues often correlates with enhanced antibacterial activity, it can also lead to increased hemolytic activity [117], which was not observed in vivo for QBP1. QBP1's phenylalanine-rich sequence may explain this effect, as phenylalanine's high hydrophobicity contributes to potent, non-toxic antimicrobial activity against both gram-positive and gram-negative bacteria [124].

With its demonstrated safety profile and ability to cross the blood-brain barrier, QBP1's antibacterial potential offers an exciting avenue for treating neurodegenerative disorders. Future research focused on amplifying QBP1's antimicrobial effects while preserving its anti-amyloidogenic properties holds the key to developing a truly innovative therapeutic solution.

4. Experimental section

4.1. Sequence-property alignment by ADAPTABLE web server

The sequence-related (SR) family of QBP1 (WKWWPGIF) was generated with the ADAPTABLE web server [67] using QBP1 as bait peptide and the following parameters: “Substitution matrix = Blosum45”; “Minimum % of similarity = 55; “ Experimentally validated = yes.” As ADAPTABLE continuously updates with new entries, sequence-related families might change slightly with time [67].

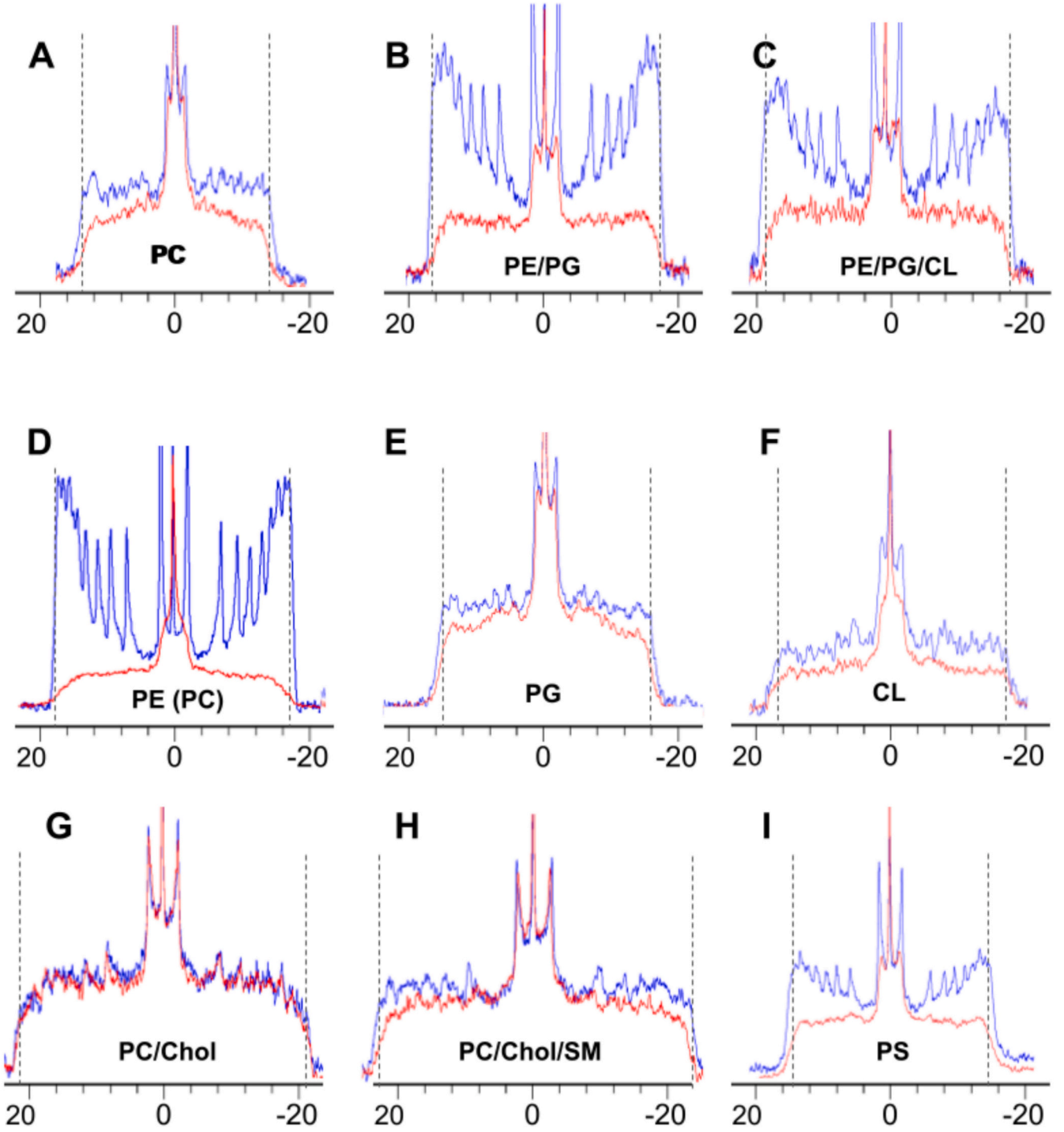

Fig. 6. Static ^{2}H NMR spectra of various MLVs in the absence (blue) and the presence (red) of QBP1 (see Experimental Section for further details on lipid composition).

4.2. Synthesis of the peptide

Fmoc(9-fluorophenylmethoxy)-amino acids, Fmoc-Rink Amide AM resin (0.64 mmol/g, particle size: 100–200 mesh) was purchased from Iris Biotech (Germany). The other chemical compounds were purchased from VWR Chemicals, Iris Biotech, or Acros and used without further purification. The peptide was synthesized on a CEM Liberty 1 microwave peptide synthesizer using standard automated continuous-flow microwave solid-phase peptide synthesis methods. A 5-fold molar excess of the above amino acids was used in a typical coupling reaction. Fmoc-deprotection was accomplished by treatment with 20 % (v/v) piperidine in N-methyl-2-pyrrolidone (NMP) at 75 °C. The coupling reaction was achieved by treatment with 2-(1H-benzotriazol-1-yl)-1,1,3,3-tetramethyluronium hexafluorophosphate (HBTU) and N,N-diisopropylethylamine (DIEA) in NMP using a standard microwave protocol (75 °C). The N-terminal acetylation was accomplished by treatment with acetic anhydride at 75 °C. The peptide was cleaved and side-chain deprotected by treatment of the peptide resin with a mixture of 3.7 ml of trifluoroacetic acid (TFA), 200 μl of triisopropylsilane, and 100 μl of H_2O during 3.5 h at room temperature. The solid support was

Table 1
Minimal inhibitory concentrations < 128 mg/L displayed by QBP1-NH_2 peptide towards different microorganisms (higher MICs and Ac-QBP1-NH_2 in Table S2).

Species	Strain/ Position	QBP1-NH_2 MIC (mg/L) MHB
Escherichia coli	DSM 1103	64
Staphylococcus aureus	CIP 103429	64
Staphylococcus aureus	NCTC12493	64
Bacillus cereus	Clinical isolate	32
Bacillus mojavensis	Clinical isolate	8
Bacillus mojavensis	0104G10	16
Enterococcus faecalis	CIP 103214	16
Staphylococcus epidermidis Methicillin-sensitive	78A5	64
Micrococcus luteus	80B1	8
Micrococcus luteus	82H5	8
Candida sp. 1049612–1	Clinical isolate	4
Candida sp.	DEL	32
Candida sp.	FOL	64

removed by filtration, the filtrate concentrated under reduced pressure, and the peptide precipitated from diethyl ether. The precipitate was washed several times with diethyl ether and dried under reduced pressure. The peptides were purified on an RP-HPLC C18 column (Phenomenex® C18, Jupiter 4 μ Proteo, 90 Å, 250 × 21.20 mm) using a mixture of aqueous 0.1 % (v/v) TFA (A) and 0.1 % (v/v) TFA in acetonitrile (B) as the mobile phase (flow rate of 3 ml/min) and employing UV detection at 210 and 254 nm (Fig. S26).

Peptides with the sequences Ac-WKWWPGIF-NH_2 and WKWWPGIF-NH_2 were obtained starting from the Fmoc-Rink Amide AM resin (145.5 mg, 0.100 mmol) as a white powder with a total yield of 29.98 % after purification by reverse-phase HPLC (analytical purity 97.6 % and 100 %, respectively, Fig. S26, supporting information).

4.3. Molecular dynamics simulations

Systems for simulations were prepared using CHARMM-GUI [125]. A total of 128 lipid molecules were placed in each lipid bilayer (i.e., 64 lipids in each leaflet), and peptide molecules were placed over the upper leaflet at a non-interacting distance (>10 Å). Lysine residue was protonated. The initial peptide structure was the one obtained by solution NMR in previous studies [56]. Acetylation of the N-terminus and amidation of the C-terminus were achieved via the CHARMM terminal group patching functionality, which is fully integrated into the CHARMM-GUI workflow. A water layer of 50-Å thickness was added above and below the lipid bilayer, which resulted in about 15,000 water molecules (30,000 in the case of cardiolipin (CL)) with small variations depending on the nature of the membrane. Systems were neutralized with Na^+ or Cl^- counterions.

MD simulations were performed using GROMACS software [126] and the CHARMM36m force field [127] under semi-isotropic NPT conditions. The TIP3P model [128] was used to describe water molecules. Each system was energy minimized with a steepest-descent algorithm for 5000 steps. Systems were equilibrated with the Berendsen barostat [129] and the Parrinello-Rahman barostat [130,131] was used to maintain pressure (1 bar) semi-isotropically with a time constant of 5 ps and a compressibility of 4.5×10^{-5} bar^{-1}. The Nose-Hoover thermostat [132,133] was chosen to maintain the systems at 310 K with a time constant of 1 ps. All bonds were constrained using the LINear Constraint Solver (LINCS) algorithm, which allowed an integration step of 2 fs. PBC (periodic boundary conditions) were employed for all simulations, and the particle mesh Ewald (PME) method [134] was used for long-range electrostatic interactions. After the standard CHARMM-GUI minimization and equilibration steps [135] the production run was performed for 500 ns, and the whole process (minimization, equilibration, and production run) was repeated once in the absence of peptide and twice in its presence. Convergence was assessed using RMSD and polar contact analysis [136].

All MD trajectories were analyzed using GROMACS tools and Fatslim [137]. gmx_MMPBSA was used to perform the end-state free energy calculations [138]. MOLMOL [139] and VMD [140] were used for visualization. Graphs and images were produced with GNUplot [141] and PyMol [142].

Binding free energies were evaluated by the gmx_MMPBSA tool [138] using the generalized Born (GB) model to evaluate the affinity of the peptide with the different membrane bilayer systems. 1000 snapshots from the last 50 ns of each simulation were analyzed by the GB^{OBC2} model (igb = 5) [143,144].

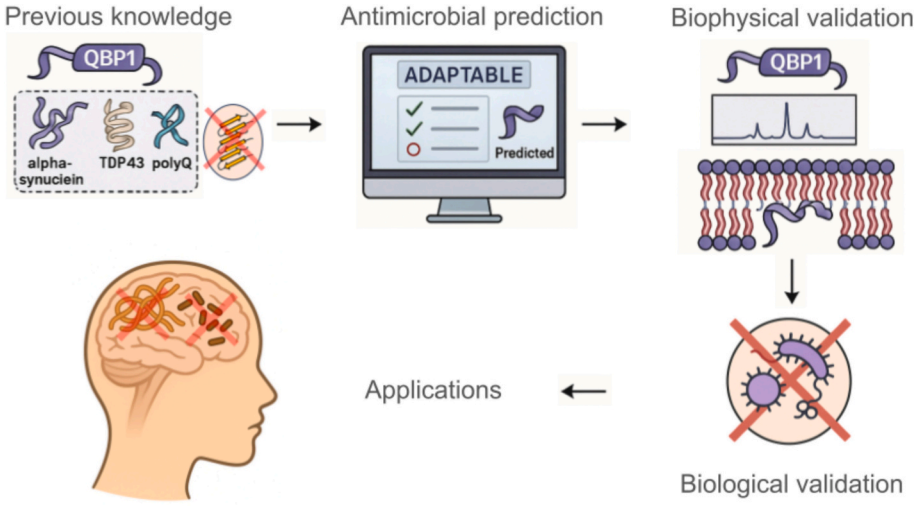

Fig. 7. Summary of the central message of our study: the potential of antimicrobial prediction tools in uncovering novel functionalities of known peptides. Starting from computational simulations, we identified a previously unrecognized antimicrobial activity in the anti-amyloidogenic QBP1 peptide. This prediction was then validated experimentally and further investigated through biophysical techniques such as NMR and MD simulations, allowing us to propose a plausible mechanism of action, at least at the level of the microbial membrane. Remarkably, the additional antimicrobial properties of QBP1 suggest a promising new avenue for targeting cerebral infections—offering a compelling perspective for the treatment of neurodegenerative disorders where infection and inflammation may play a contributing role.

4.4. Human cell origin and culture

4.4.1. Ethics and origin of the human cells

Human brain pericytes (HBPs) were kindly provided by Dr. Fumitaka Shimizu and Pr. Takashi Kanda from the Department of Neurology and Clinical Neuroscience, Graduate School of Medicine, Yamaguchi University, Ube, Japan. HBPs were isolated from a patient who had suddenly died from a heart attack [145]. The study protocol for human tissue was approved by the ethics committee of the Medical Faculty (IRB#: H18–033-6), University of Yamaguchi Graduate School, and was conducted in accordance with the Declaration of Helsinki, as amended in Somerset West in 1996. For the $CD34^+$-hematopoietic stem cells, written informed consent was obtained from the family of the participant before enrollment in the study.

The collection of human umbilical cord blood requires that infants' parents sign consent forms in compliance with French legislation. The protocol was approved by the French Ministry of Higher Education and Research (CODECOH, Number DC2011–1321). All experiments were carried out in accordance with the approved protocol. HBPs and $CD34^+$-hematopoietic stem cells were regularly checked for mycoplasma contamination, and short tandem repeat (STR) analysis confirmed the absence of cross-contamination. According to French legislation, human cells were handled in the laboratory under agreement number L2–1235. $CD34^+$-hematopoietic stem cells were isolated from human umbilical cord blood and differentiated into ECs ($CD34^+$-ECs) as previously described [146]. $CD34^+$-ECs were seeded in 100 mm 1 % gelatin-coated dishes containing complete Endothelial Cell Growth Medium MV2 (ECGMV2, PromoCell GmbH (Heidelberg, Germany)) supplemented with 0.5 % gentamicin. The HBPs were grown in Dulbecco's modified Eagle medium (DMEM, Sigma) supplemented with 4.5 g/L D-glucose, 10 % FBS, 1 % L-glutamine, and 1 % penicillin-streptomycin, as previously described [146].

4.4.2. In vitro BBB model

The BBB model was prepared as previously published [146,147]. Briefly, $CD34^+$-ECs (8×10^4 cells/insert) were seeded into Matrigel™-coated filters (Costar Transwell inserts, pore size 0.4 μm, Corning SAS, Avon, France). Then, the inserts were placed in collagen-coated 12-well plates containing HBPs (5×10^4 cells/well). After 5 days of co-culture, $CD34^+$-ECs acquire the major BBB properties observed in vivo and reproduce a suitable model for investigating BBB permeability and physiology [97,148–151]. HBPs were also deeply characterized in our previous studies [152]. The upper compartment represents the apical side of the model (blood), and the lower side represents the basolateral compartment (brain). Once differentiated, endothelial cells were treated, and permeability studies and sample collection were subsequently performed as described below.

4.5. Permeability assays

Cells were treated with 5 or 50 μM of QBP1 incubated into the luminal side of the human BBB model for 24 h. Permeability assays were then performed as previously described [153]. Ringer–HEPES (RH buffer) buffer (150 mM NaCl, 5.2 mM KCl, 2.2 mM $CaCl_2$, 0.2 mM $MgCl_2$, 6 H_2O, 6 mM $NaHCO_3$, 5 mM HEPES, pH 7.4) at 37 °C was added to empty wells in a 12-well plate (Costar). Filter inserts containing BBB endothelial cells were subsequently transferred to a 12-well plate and filled with RH containing the fluorescent integrity marker sodium fluorescein (NaFlu; 10 μM; Life Technologies, Carlsbad, CA, USA), which poorly crosses the BBB. After 1 h, the filter inserts were withdrawn from the receiver compartment. Aliquots from the donor solution were taken at the beginning and the end of the experiments, and the fluorescence was quantified using a microplate reader (Synergy H1 multiplate reader, BioTek Instruments SAS, Colmar, France) at an excitation wavelength (λ) of 490 nm and an emission wavelength of 525 nm. The permeability coefficient was then calculated as previously described [153]. Briefly, both the insert permeability (PSf, for inserts only coated with Matrigel™) and the permeability of inserts containing BBB endothelial cells (PSt, for inserts with Matrigel™ and cells) were considered according to the following formula: $1/PSe = 1/PSt - 1/PSf$. The permeability value of the BBB endothelial monolayer was then divided by the surface area of the insert (1.12 cm^2) to obtain the permeability coefficient (Pe) of each molecule (at 10^{-3} cm/min).

4.6. Immunofluorescence labeling of the tight junctions

BBB endothelial cells were fixed with ice-cold methanol (20 s) for CLAUDIN-5 labeling or cold paraformaldehyde (PFA) 4 % (10 min) for ZONULA OCCLUDENS 1 (ZO-1) and rinsed twice with cold calcium- and magnesium-free PBS (PBS-CMF; 8 g/L NaCl, 0.2 g/L KCl, 0.2 g/L KH_2PO_4, 2.86 g/L $Na_2HPO_4{\cdot}12\ H_2O$; pH 7.4). A step of 10 min-permeabilization (10 min at room temperature (RT)) with 0.1 % Triton X-100 in PBS-CMF was required for PFA-fixed samples. Unspecific binding was blocked (30 min, RT) using a sea block buffer solution (SBBS, Thermo Fisher Scientific). Then, the cells were incubated (60 min, RT) with primary antibodies against CLAUDIN-5 (1:100, Invitrogen, 34–1600) or ZO-1 (1:200, Invitrogen, 61–7300) in PBS-CMF containing 5 % (v/v) SBBS (PBS-SBBS). After rinsing, the cells were incubated (30 min, RT) with a secondary polyclonal antibody (Life Technologies, A-11034) and 10 ng/mL DAPI (Invitrogen, D1306) for nuclear staining in PBS-SBBS. After rising, the cells were mounted using ProLong Gold Antifade Mountant (Thermo Fisher Scientific). Images were acquired using a Leica microscope (DMi8, Leica Microsystems SAS, Nanterre, France) and processed using ImageJ software (National Institutes of Health, Bethesda, MD, USA).

4.7. Solid-state NMR experiments

The lipids for the experiments were purchased from Avanti Polar Lipids (Alabaster, AL, USA). Multilamellar vesicles (MLVs) were prepared according to the usual procedures with lipids containing deuterated palmitoyl chains [154] using the following molar proportions: 50 %:50 % POPC/POPC:d31, 50 %:50 % POPG/POPG:d31, 70 %:30 % POPE:d31/POPG, 50 %:50 % CL/POPC:d31, 70 %:30 % POPE:d31/POPC, 70 %:30 % POPC:d31/Cholesterol, 35 %:35 %:30 % POPC:d31/eggSM/Cholesterol. Lipids were solubilized in chloroform and mixed in order to obtain the desired proportions, leading to a total lipid concentration of 60 mM. The resulting sample was evaporated under nitrogen steam, hydrated, and lyophilized overnight to remove traces of the solvent. The resulting powder was hydrated with 80 μl of Milli-Q water (for non-charged lipids) or 50 mM phosphate buffer pH 6.6 and 100 mM NaCl (for charged lipids). Samples were vortexed and homogenized using four freeze-thaw cycles of freezing (−80 °C, 15 min) followed by thawing (42 °C, 15 min). The MLV samples were then inserted in a 7-mm ssNMR rotor to perform the experiments. 2.4 mM of QBP1 peptide was added for the study of the interaction.

ssNMR experiments were performed at 310 K on a Bruker Avance Biospin 300 WB (7.05 T) equipped with a CP-MAS 7-mm probe. Static ^2H NMR was carried out using a phase-cycled quadrupolar echo pulse sequence (90°x-τ-90°y-τ-acq) [155]. The used parameters were a π/2 pulse of 5.4 μs, an interpulse delay of 40 μs, a recycled delay of 1.5 s, and a number of acquisitions ranging from 8 k to 14 k depending on samples. An exponential line broadening of 100 Hz was applied before the Fourier transform from the top of the echo signal.

4.8. Susceptibility testing

Susceptibility testing by the broth microdilution technique was performed in triplicate according to CLSI guidelines [156]. Inocula were prepared in sterile water solution and standardized using a nephelometer (Vitek Densicheck, Biomérieux), then diluted in the appropriate media to obtain a final solution of around 5×10^5 CFU/mL in Mueller-

Hinton Broth (MHB) and cation-adjusted Mueller-Hinton Broth (CA-MHB). 96 round-bottom microplates were incubated statically for 18–24 h at 37 °C. Amikacin (in water) and ciprofloxacin (in DMSO) stock solutions were used as controls in each series of experiments, and results were compared with CLSI ranges. The activities of the peptides were determined for high concentrations ranging from 0.25 to 256 mg/L. The MIC was determined as the lowest concentration at which wells remained visually clear.

The evaluated strains (specified in tables with activity results) were precharacterized and provided by Deutsche Sammlung für Mikroorganismen (Braunschweig, Germany), Institut Pasteur (Paris, France), Bicêtre Hospital (Paris, France), and the German National Reference Centre for Multidrug-resistant Gram-negative Bacteria (Bochum, Germany).

Abbreviations

HDPs	host defense peptides
AMPs	antimicrobial peptides
NMP	N-methyl-2-pyrrolidone
HBTU	2-(1H-benzotriazol-1-yl)-1,1,3,3-tetramethyluronium hexafluorophosphate
DIEA	N,N-diisopropylethylamine
TFA	trifluoroacetic acid
PE	phosphatidylethanolamine
PG	phosphatidylglycerol
PI	phosphatidylinositol
PS	phosphatidylserine
CL	cardiolipin
NPT	isothermal-isobaric ensemble
LINCS	LINear Constraint Solver
PBC	Periodic Boundary Conditions
PME	particle mesh Ewald
RMSD	root-mean-square deviation
POPC	1-palmitoyl-2-oleoyl-glycero-3-phosphocholine
POPG	1-palmitoyl-2-oleoyl-sn-glycero-3-phospho-(1′-rac-glycerol)
POPS	1-palmitoyl-2-oleoyl-sn-glycero-3-phospho-L-serine
POPE	1-palmitoyl-2-oleoyl-sn-glycero-3-phosphoethanolamine
POPI	1-palmitoyl-2-oleoyl-sn-glycero-3-phosphoinositol
MIC	minimal inhibitory concentration
ADAPTABLE	All-in-one Database of Antimicrobial Peptides clusTered in fAmilies for Boosted seLectivity and dEsign
SR	sequence-related family
CHOL	cholesterol
ERGO	ergosterol

CRediT authorship contribution statement

Francisco Ramos-Martín: Writing – review & editing, Writing – original draft, Visualization, Validation, Software, Methodology, Investigation, Formal analysis, Data curation, Conceptualization. **François Peltier:** Writing – review & editing, Validation, Methodology, Investigation, Formal analysis, Data curation. **Saoussen Oueslati:** Writing – review & editing, Validation, Methodology, Investigation, Formal analysis, Data curation. **Liam Cousin:** Methodology, Formal analysis. **Mariam Rima:** Writing – review & editing, Validation, Methodology, Investigation, Formal analysis. **Marie Perret:** Writing – review & editing, Methodology, Investigation, Formal analysis. **Laurie Bibens:** Investigation. **Emmanuel Sevin:** Methodology, Formal analysis. **Viviane Antonietti:** Writing – review & editing, Validation, Methodology, Investigation, Formal analysis. **Sophie Da Nascimento:** Validation, Investigation. **Catherine Sarazin:** Writing – review & editing, Resources, Project administration, Funding acquisition. **Fabien Gosselet:** Writing – review & editing, Resources, Project administration, Funding acquisition, Conceptualization. **Thierry Naas:** Validation, Supervision, Resources, Project administration, Methodology. **Pascal Sonnet:** Writing – review & editing, Validation, Supervision, Resources, Project administration, Methodology, Funding acquisition, Formal analysis, Conceptualization. **Nicola D'Amelio:** Writing – review & editing, Writing – original draft, Visualization, Validation, Supervision, Resources, Project administration, Methodology, Investigation, Funding acquisition, Formal analysis, Conceptualization.

Funding

Francisco Ramos-Martín's PhD scholarship was co-funded by Conseil régional des Hauts-de-France and by the European Fund for Economic and Regional Development (ERDF). As part of the CPER MOSOPS, this project has received financial support from the French State, Région Hauts-de-France, INSERM, and the A2U Alliance's universities (Artois/UPJV/ULCO).

Declaration of competing interest

The authors declare that they have no known competing financial interests or personal relationships that could have appeared to influence the work reported in this paper.

Acknowledgements

We thank the Matrics platform at the University of "Picardie Jules Verne" and the "Méso-centre de Calcul Scientifique Intensif" at the University of Lille for providing computing resources. We thank Dr. Fumitaka Shimizu and Pr. Takashi Kanda from the Department of Neurology and Clinical Neuroscience, Graduate School of Medicine, Yamaguchi University, for kindly providing the human brain pericytes (HBPs). We finally thank Aurélie Herrero for her help on antimicrobial tests.

Appendix A. Supplementary data

Supplementary data to this article can be found online at https://doi.org/10.1016/j.ijbiomac.2025.144938.

References

[1] R. Hervás, J. Oroz, A. Galera-Prat, O. Goñi, A. Valbuena, A.M. Vera, A. Gómez-Sicilia, F. Losada-Urzáiz, V.N. Uversky, M. Menéndez, D.V. Laurents, M. Bruix, M. Carrión-Vázquez, Common features at the start of the neurodegeneration cascade, PLoS Biol. 10 (2012) e1001335.
[2] M. Mompean, D.V. Laurents, Intrinsically disordered domains, amyloids and protein liquid phases: evolving concepts and open questions, Protein Pept. Lett. 24 (2017) 281–293.
[3] T.D.N. Luong, S. Nagpal, M. Sadqi, V. Muñoz, A modular approach to map out the conformational landscapes of unbound intrinsically disordered proteins, Proc. Natl. Acad. Sci. USA 119 (2022) e2113572119.
[4] S.M. Butterfield, H.A. Lashuel, Amyloidogenic protein-membrane interactions: mechanistic insight from model systems, Angew. Chem. Int. Ed. Engl. 49 (2010) 5628–5654.
[5] T. Takahashi, S. Kikuchi, S. Katada, Y. Nagai, M. Nishizawa, O. Onodera, Soluble polyglutamine oligomers formed prior to inclusion body formation are cytotoxic, Hum. Mol. Genet. 17 (2008) 345–356.
[6] P.C. Ke, M.-A. Sani, F. Ding, A. Kakinen, I. Javed, F. Separovic, T.P. Davis, R. Mezzenga, Implications of peptide assemblies in amyloid diseases, Chem. Soc. Rev. 46 (2017) 6492–6531.
[7] R. Hervás, L. Li, A. Majumdar, M.D.C. Fernández-Ramírez, J.R. Unruh, B. D. Slaughter, A. Galera-Prat, E. Santana, M. Suzuki, Y. Nagai, M. Bruix, S. Casas-Tintó, M. Menéndez, D.V. Laurents, K. Si, M. Carrión-Vázquez, Molecular basis of Orb2 Amyloidogenesis and blockade of memory consolidation, PLoS Biol. 14 (2016) e1002361.
[8] J. Oroz, S.S. Félix, E.J. Cabrita, D.V. Laurents, Structural transitions in Orb2 prion-like domain relevant for functional aggregation in memory consolidation, J. Biol. Chem. 295 (2020), https://doi.org/10.1074/jbc.RA120.015211.
[9] R.R. Nair, J.K. Johnson, Prions and neuro degenerative diseases, Afr. J. Biotechnol. 10 (2011) 2366–2374.
[10] E. Lopez-Rodriguez, J. Pérez-Gil, Structure-function relationships in pulmonary surfactant membranes: from biophysics to therapy, Biochim. Biophys. Acta 1838 (2014) 1568–1585.

[11] P.K. Auluck, G. Caraveo, S. Lindquist, A-Synuclein: membrane interactions and toxicity in Parkinson's disease, Annu. Rev. Cell Dev. Biol. 26 (2010), https://doi.org/10.1146/annurev.cellbio.042308.113313.

[12] M. Zhang, J. Zhao, J. Zheng, Molecular understanding of a potential functional link between antimicrobial and amyloid peptides, Soft Matter 10 (2014) 7425–7451.

[13] P.K.J. Kinnunen, Amyloid formation on lipid membrane surfaces, Open Biol. J. 2 (2009). https://benthamopen.com/ABSTRACT/TOBIOJ-2-163.

[14] F. Harris, S.R. Dennison, D.A. Phoenix, Aberrant action of amyloidogenic host defense peptides: a new paradigm to investigate neurodegenerative disorders? FASEB J. 26 (2012) 1776–1781.

[15] A. Naito, N. Matsumori, A. Ramamoorthy, Dynamic membrane interactions of antibacterial and antifungal biomolecules, and amyloid peptides, revealed by solid-state NMR spectroscopy, Biochim. Biophys. Acta Gen. Subj. 2018 (1862) 307–323.

[16] N.B. Last, A.D. Miranker, Common mechanism unites membrane poration by amyloid and antimicrobial peptides, Proc. Natl. Acad. Sci. USA 110 (2013) 6382–6387.

[17] J. Greenwald, R. Riek, Biology of amyloid: structure, function, and regulation, Structure 18 (2010), https://doi.org/10.1016/j.str.2010.08.009.

[18] D.M. Fowler, A.V. Koulov, W.E. Balch, J.W. Kelly, Functional amyloid–from bacteria to humans, Trends Biochem. Sci. 32 (2007), https://doi.org/10.1016/j.tibs.2007.03.003.

[19] O.V. Galzitskaya, S.R. Kurpe, A.V. Panfilov, A.V. Glyakina, S.Y. Grishin, A. P. Kochetov, E.I. Deryusheva, A.V. Machulin, S.V. Kravchenko, P.A. Domnin, A. K. Surin, V.N. Azev, S.A. Ermolaeva, Amyloidogenic peptides: new class of antimicrobial peptides with the novel mechanism of activity, Int. J. Mol. Sci. 23 (2022) 5463.

[20] S.J. Soscia, J.E. Kirby, K.J. Washicosky, S.M. Tucker, M. Ingelsson, B. Hyman, M. A. Burton, L.E. Goldstein, S. Duong, R.E. Tanzi, R.D. Moir, The Alzheimer's disease-associated amyloid beta-protein is an antimicrobial peptide, PLoS One 5 (2010) e9505.

[21] M.M. Welling, R.J.A. Nabuurs, L. van der Weerd, Potential role of antimicrobial peptides in the early onset of Alzheimer's disease, Alzheimers Dement. 11 (2015) 51–57.

[22] D.A. Phoenix, F. Harris, M. Mura, S.R. Dennison, The increasing role of phosphatidylethanolamine as a lipid receptor in the action of host defence peptides, Prog. Lipid Res. 59 (2015) 26–37.

[23] C.S. Little, C.J. Hammond, A. MacIntyre, B.J. Balin, D.M. Appelt, Chlamydia pneumoniae induces Alzheimer-like amyloid plaques in brains of BALB/c mice, Neurobiol. Aging 25 (2004) 419–429.

[24] J. Doorduin H.C. Klein de J.R. Jong R.A. Dierckx de E.F. Vries Evaluation of [11C]-DAA1106 for imaging and quantification of neuroinflammation in a rat model of herpes encephalitis Nucl. Med. Biol. 37 2010 https://doi.org/10.1016/j.nucmedbio.2009.09.002.

[25] Q. Qin, Y. Li, Herpesviral infections and antimicrobial protection for Alzheimer's disease: implications for prevention and treatment, J. Med. Virol. 91 (2019) 1368–1377.

[26] L.C. Norins, The beehive theory: role of microorganisms in late sequelae of traumatic brain injury and chronic traumatic encephalopathy, Med. Hypotheses 128 (2019) 1–5.

[27] A.Y. Vittor, M. Long, P. Chakrabarty, L. Aycock, V. Kollu, S.T. DeKosky, West Nile virus-induced neurologic sequelae-relationship to neurodegenerative cascades and dementias, Curr. Trop. Med. Rep. 7 (2020) 25–36.

[28] E. Caggiu, G. Arru, S. Hosseini, M. Niegowska, G. Sechi, I.R. Zarbo, L.A. Sechi, Inflammation, infectious triggers, and Parkinson's disease, Front. Neurol. 10 (2019) 122.

[29] N. Limphaibool, P. Iwanowski, M.J.V. Holstad, D. Kobylarek, W. Kozubski, Infectious etiologies of parkinsonism: Pathomechanisms and clinical implications, Front. Neurol. 10 (2019) 652.

[30] D. Matheoud, T. Cannon, A. Voisin, A.-M. Penttinen, L. Ramet, A.M. Fahmy, C. Ducrot, A. Laplante, M.-J. Bourque, L. Zhu, R. Cayrol, A. Le Campion, H. M. McBride, S. Gruenheid, L.-E. Trudeau, M. Desjardins, Intestinal infection triggers Parkinson's disease-like symptoms in Pink1−/− mice, Nature 571 (2019) 565–569.

[31] M. Linard, A. Ravier, L. Mougué, I. Grgurina, A.-L. Boutillier, A. Foubert-Samier, F. Blanc, C. Helmer, Infectious agents as potential drivers of α-Synucleinopathies, Mov. Disord. 37 (2022) 464–477.

[32] S. Voth, M. Gwin, C.M. Francis, R. Balczon, D.W. Frank, J.-F. Pittet, B. M. Wagener, S.A. Moser, M. Alexeyev, N. Housley, J.P. Audia, S. Piechocki, K. Madera, A. Simmons, M. Crawford, T. Stevens, Virulent Pseudomonas aeruginosa infection converts antimicrobial amyloids into cytotoxic prions, FASEB J. 34 (2020) 9156–9179.

[33] C.-S. Choi, M. Gwin, S. Voth, C. Kolb, C. Zhou, A.R. Nelson, A. deWeever, A. Koloteva, N.S. Annamdevula, J.M. Murphy, B.M. Wagener, J.-F. Pittet, S.-T. S. Lim, R. Balczon, T. Stevens, M.T. Lin, Cytotoxic tau released from lung microvascular endothelial cells upon infection with Pseudomonas aeruginosa promotes neuronal tauopathy, J. Biol. Chem. 298 (2022) 101482.

[34] Z. Rahic, E. Buratti, S. Cappelli, Reviewing the potential links between viral infections and TDP-43 Proteinopathies, Int. J. Mol. Sci. 24 (2023) 1581, https://doi.org/10.3390/ijms24021581.

[35] K. Berstad, J.E.R. Berstad, Parkinson's disease; the hibernating spore hypothesis, Med. Hypotheses 104 (2017), https://doi.org/10.1016/j.mehy.2017.05.022.

[36] M. Laurence, J. Benito-León, F. Calon, Malassezia and Parkinson's disease, Front. Neurol. 10 (2019), https://doi.org/10.3389/fneur.2019.00758.

[37] D. Pisa, R. Alonso, L. Carrasco, Parkinson's disease: a comprehensive analysis of Fungi and Bacteria in brain tissue, Int. J. Biol. Sci. 16 (2020) 1135.

[38] N. Kobayashi, J. Masuda, J. Kudoh, N. Shimizu, T. Yoshida, Binding sites on tau proteins as components for antimicrobial peptides, Biocontrol Sci. 13 (2008) 49–56.

[39] M. Pasupuleti, M. Roupe, V. Rydengård, K. Surewicz, W.K. Surewicz, A. Chalupka, M. Malmsten, O.E. Sörensen, A. Schmidtchen, Antimicrobial activity of human prion protein is mediated by its N-terminal region, PLoS One 4 (2009) e7358.

[40] R. Lathe, J.-L. Darlix, Prion protein PRNP: a new player in innate immunity? The Aβ connection, J. Alzheimers Dis. Rep. 1 (2017) 263–275.

[41] M.F.M. Sciacca, J.R. Brender, D.-K. Lee, A. Ramamoorthy, Phosphatidylethanolamine enhances amyloid fiber-dependent membrane fragmentation, Biochemistry 51 (2012) 7676–7684.

[42] L. Wang, Q. Liu, J.-C. Chen, Y.-X. Cui, B. Zhou, Y.-X. Chen, Y.-F. Zhao, Y.-M. Li, Antimicrobial activity of human islet amyloid polypeptides: an insight into amyloid peptides' connection with antimicrobial peptides, Biol. Chem. 393 (2012) 641–646.

[43] S.-C. Park, J.C. Moon, S.Y. Shin, H. Son, Y.J. Jung, N.-H. Kim, Y.-M. Kim, M.-K. Jang, J.R. Lee, Functional characterization of alpha-synuclein protein with antimicrobial activity, Biochem. Biophys. Res. Commun. 478 (2016) 924–928.

[44] C.T. Tulisiak, G. Mercado, W. Peelaerts, L. Brundin, P. Brundin, Can infections trigger alpha-synucleinopathies? Prog. Mol. Biol. Transl. Sci. 168 (2019) https://doi.org/10.1016/bs.pmbts.2019.06.002.

[45] J.J. Tomlinson, B. Shutinoski, L. Dong, F. Meng, D. Elleithy, N.A. Lengacher, A. P. Nguyen, G.O. Cron, Q. Jiang, E.D. Roberson, R.L. Nussbaum, N.K. Majbour, O. M. El-Agnaf, S.A. Bennett, D.C. Lagace, J.M. Woulfe, S. Sad, E.G. Brown, M. G. Schlossmacher, Holocranohistochemistry enables the visualization of α-synuclein expression in the murine olfactory system and discovery of its systemic anti-microbial effects, J. Neural Transm. 124 (2017) 721–738.

[46] O. Cañadas, B. Olmeda, A. Alonso, J. Pérez-Gil, Lipid-protein and protein-protein interactions in the pulmonary surfactant system and their role in lung homeostasis, Int. J. Mol. Sci. 21 (2020), https://doi.org/10.3390/ijms21103708.

[47] S.W. Glasser, J.E. Baatz, T.R. Korfhagen, Surfactant protein-C in the maintenance of lung integrity and function, J Allergy Ther 7 (2011) 001.

[48] L. Zhu, R. Maruvada, A. Sapirstein, K.U. Malik, M. Peters-Golden, K.S. Kim, Arachidonic acid metabolism regulates Escherichia coli penetration of the blood-brain barrier, Infect. Immun. 78 (2010) 4302–4310.

[49] H. Wang, X. Liu, C. Tan, W. Zhou, J. Jiang, W. Peng, X. Zhou, L. Mo, L. Chen, Bacterial, viral, and fungal infection-related risk of Parkinson's disease: Meta-analysis of cohort and case–control studies, Brain Behav. 10 (2020), https://doi.org/10.1002/brb3.1549.

[50] R.C. Green, L.S. Schneider, D.A. Amato, A.P. Beelen, G. Wilcock, E.A. Swabb, K. H. Zavitz, Tarenflurbil phase 3 study group, effect of tarenflurbil on cognitive decline and activities of daily living in patients with mild Alzheimer disease: a randomized controlled trial, JAMA 302 (2009) 2557–2564.

[51] D. Dominguez, J. Tournoy, D. Hartmann, T. Huth, K. Cryns, S. Deforce, L. Serneels, I.E. Camacho, E. Marjaux, K. Craessaerts, A.J.M. Roebroek, M. Schwake, R. D'Hooge, P. Bach, U. Kalinke, D. Moechars, C. Alzheimer, K. Reiss, P. Saftig, B. De Strooper, Phenotypic and biochemical analyses of BACE1- and BACE2-deficient mice, J. Biol. Chem. 280 (2005) 30797–30806.

[52] D.K.V. Kumar, S.H. Choi, K.J. Washicosky, W.A. Eimer, S. Tucker, J. Ghofrani, A. Lefkowitz, G. McColl, L.E. Goldstein, R.E. Tanzi, R.D. Moir, Amyloid-β peptide protects against microbial infection in mouse and worm models of Alzheimer's disease, Sci. Transl. Med. 8 (2016) 340ra72.

[53] Y. Nagai, T. Tucker, H. Ren, D.J. Kenan, B.S. Henderson, J.D. Keene, W. J. Strittmatter, J.R. Burke, Inhibition of polyglutamine protein aggregation and cell death by novel peptides identified by phage display screening, J. Biol. Chem. 275 (2000) 10437–10442.

[54] M.F. Perutz, T. Johnson, M. Suzuki, J.T. Finch, Glutamine repeats as polar zippers: their possible role in inherited neurodegenerative diseases, Proc. Natl. Acad. Sci. USA 91 (1994) 5355–5358.

[55] L. Hamuro, G. Zhang, T.J. Tucker, C. Self, W.J. Strittmatter, J.R. Burke, Optimization of a polyglutamine aggregation inhibitor peptide (QBP1) using a thioflavin T fluorescence assay, Assay Drug Dev. Technol. 5 (2007) 629–636.

[56] F. Ramos-Martín, R. Hervás, M. Carrión-Vázquez, D.V. Laurents, NMR spectroscopy reveals a preferred conformation with a defined hydrophobic cluster for polyglutamine binding peptide 1, Arch. Biochem. Biophys. 558 (2014) 104–110.

[57] Y. Nagai, N. Fujikake, K. Ohno, H. Higashiyama, H.A. Popiel, J. Rahadian, M. Yamaguchi, W.J. Strittmatter, J.R. Burke, T. Toda, Prevention of polyglutamine oligomerization and neurodegeneration by the peptide inhibitor QBP1 in Drosophila, Hum. Mol. Genet. 12 (2003) 1253–1259.

[58] P.O. Bauer, A. Goswami, H.K. Wong, M. Okuno, M. Kurosawa, M. Yamada, H. Miyazaki, G. Matsumoto, Y. Kino, Y. Nagai, N. Nukina, Harnessing chaperone-mediated autophagy for the selective degradation of mutant huntingtin protein, Nat. Biotechnol. 28 (2010) 256–263.

[59] P.A. Egorova, I.B. Bezprozvanny, Molecular mechanisms and therapeutics for spinocerebellar Ataxia type 2, Neurotherapeutics 16 (2019) 1050–1073.

[60] M. Mompeán, D. Ramírez de Mingo, R. Hervás, M.D.C. Fernández-Ramírez, M. Carrión-Vázquez, D.V. Laurents, Molecular mechanism of the inhibition of TDP-43 amyloidogenesis by QBP1, Arch. Biochem. Biophys. 675 (2019) 108113.

[61] R. Hervás, M. del Carmen Fernández-Ramírez, A. Galera-Prat, M. Suzuki, Y. Nagai, M. Bruix, M. Menéndez, D.V. Laurents, M. Carrión-Vázquez, Divergent CPEB prion-like domains reveal different assembly mechanisms for a generic amyloid-like fold, BMC Biol. 19 (2021) 1–14.

[62] Q. Zhang, H. Tsoi, S. Peng, P.P. Li, K.-F. Lau, D.D. Rudnicki, J.C.-K. Ngo, H.Y. E. Chan, Assessing a peptidylic inhibitor-based therapeutic approach that simultaneously suppresses polyglutamine RNA- and protein-mediated toxicities in patient cells and Drosophila, Dis. Model. Mech. 9 (2016) 321–334.

[63] E.N. Minakawa, Y. Nagai, Protein aggregation inhibitors as disease-modifying therapies for Polyglutamine diseases, Front. Neurosci. 15 (2021), https://doi.org/10.3389/fnins.2021.621996.

[64] M. Yang, Q. Zhang, Q. Wang, K.K. Sørensen, J.T. Boesen, S.Y. Ma, K.J. Jensen, K. M. Kwan, J.C.K. Ngo, H.Y.E. Chan, Z. Zuo, Brain-targeting delivery of two Peptidylic inhibitors for their combination therapy in transgenic Polyglutamine disease mice via intranasal administration, Mol. Pharm. 15 (2018) 5781–5792.

[65] A.S. Joshi, V. Singh, A. Gahane, A.K. Thakur, Biodegradable nanoparticles containing mechanism based peptide inhibitors reduce Polyglutamine aggregation in cell models and alleviate motor symptoms in a Drosophila model of Huntington's disease, ACS Chem. Neurosci. 10 (2019) 1603–1614.

[66] L. Zuo, W. Li, J. Shi, Y. Su, H. Shuai, X. Yu, SynB3 conjugated QBP1 passes blood-brain barrier models and inhibits polyQ protein aggregation, Protein Pept. Lett. (2021), https://doi.org/10.2174/0929866529666211221163930.

[67] F. Ramos-Martín, T. Annaval, S. Buchoux, C. Sarazin, N. D'Amelio, Adaptable: a comprehensive web platform of antimicrobial peptides tailored to the user's research, Life Sci. Alliance 2 (2019), https://doi.org/10.26508/lsa.201900512.

[68] M.M. Welling, A. Paulusma-Annema, H.S. Balter, E.K. Pauwels, P.H. Nibbering, Technetium-99m labelled antimicrobial peptides discriminate between bacterial infections and sterile inflammations, Eur. J. Nucl. Med. 27 (2000) 292–301.

[69] F. Gemmel, N. Dumarey, M. Welling, Future diagnostic agents, Semin. Nucl. Med. 39 (2009), https://doi.org/10.1053/j.semnuclmed.2008.08.005.

[70] M.M. Welling, C.P.J.M. Brouwer, W. van 't Hof, E.C.I. Veerman, A.V. N. Amerongen, Histatin-derived monomeric and dimeric synthetic peptides show strong bactericidal activity towards multidrug-resistant Staphylococcus aureus in vivo, Antimicrob. Agents Chemother. 51 (2007) 3416–3419.

[71] J.E. Bernstein, S. Kashyap, K. Ray, A. Ananda, Infections in deep brain stimulator surgery, Cureus (2019), https://doi.org/10.7759/cureus.5440.

[72] R.F. Itzhaki, M.A. Wozniak, D.M. Appelt, B.J. Balin, Infiltration of the brain by pathogens causes Alzheimer's disease, Neurobiol. Aging 25 (2004) 619–627.

[73] C. Carter, Alzheimer's disease: APP, gamma secretase, APOE, CLU, CR1, PICALM, ABCA7, BIN1, CD2AP, CD33, EPHA1, and MS4A2, and their relationships with herpes simplex, C. pneumoniae, other suspect pathogens, and the immune system, International Journal of Alzheimer's Disease 2011 (2011). https://www.hindawi.com/journals/ijad/2011/501862/abs/.

[74] Y. Zheng, W. Shang, H. Peng, Y. Rao, X. Zhao, Z. Hu, Y. Yang, Q. Hu, L. Tan, K. Xiong, S. Li, J. Zhu, X. Hu, R. Zhou, M. Li, X. Rao, Virulence determinants are required for brain abscess formation through Staphylococcus aureus infection and are potential targets of Antivirulence factor therapy, Front. Microbiol. 10 (2019), https://doi.org/10.3389/fmicb.2019.00682.

[75] J. Zou, W. Shang, L. Yang, T. Liu, L. Wang, X. Li, J. Zhao, X. Rao, J. Gao, X. Fan, Microglia activation in the mPFC mediates anxiety-like behaviors caused by Staphylococcus aureus strain USA300, Brain Behav. 12 (2022) e2715.

[76] R.M. Antonello, N. Riccardi, How we deal with Staphylococcus aureus (MSSA, MRSA) central nervous system infections, Frontiers in Bioscience-Scholar 14 (2022) 1, https://doi.org/10.31083/j.fbs1401001.

[77] L.B. Astrup, K. Skovgaard, R.S. Rasmussen, T.M. Iburg, J.S. Agerholm, B. Aalbæk, H.E. Jensen, O.L. Nielsen, F.F. Johansen, P.M.H. Heegaard, P.S. Leifsson, Staphylococcus aureus infected embolic stroke upregulates Orm1 and Cxcl2 in a rat model of septic stroke pathology, Neurol. Res. 41 (2019) 399–412, https://doi.org/10.1080/01616412.2019.1573455.

[78] O. Flores-Maldonado, G.M. González, J.F. Enríquez-Bañuelos, Á. Andrade, R. Treviño-Rangel, M.A. Becerril-García, Candida albicans causes brain regional invasion and necrosis, and activation of microglia during lethal neonatal neurocandidiasis, Microbes Infect. 25 (2023) 105119.

[79] V.M. Godkhindi, V. Monappa, N.V. Kairanna, S. Sharma, G. Vasudevan, K. D. Hebbar, Brain infections that mimic malignancy, Diagn. Histopathol. 28 (2022) 456–466, https://doi.org/10.1016/j.mpdhp.2022.08.009.

[80] P. Staubitz, A. Peschel, W.F. Nieuwenhuizen, M. Otto, F. Götz, G. Jung, R.W. Jack, Structure-function relationships in the tryptophan-rich, antimicrobial peptide indolicidin, J. Pept. Sci. 7 (2001), https://doi.org/10.1002/psc.351.

[81] H.J. Schluesener, S. Radermacher, A. Melms, S. Jung, Leukocytic antimicrobial peptides kill autoimmune T cells, J. Neuroimmunol. 47 (1993), https://doi.org/10.1016/0165-5728(93)90030-3.

[82] T.S. Ryge, X. Doisy, D. Ifrah, J.E. Olsen, P.R. Hansen, New indolicidin analogues with potent antibacterial activity, J. Pept. Res. 64 (2004) 171–185.

[83] C.-W. Tsai, N.-Y. Hsu, C.-H. Wang, C.-Y. Lu, Y. Chang, H.-H.G. Tsai, R.-C. Ruaan, Coupling molecular dynamics simulations with experiments for the rational design of indolicidin-analogous antimicrobial peptides, J. Mol. Biol. 392 (2009) 837–854.

[84] J.C.Y. Hsu, C.M. Yip, Molecular dynamics simulations of indolicidin association with model lipid bilayers, Biophys. J. 92 (2007) L100–L102.

[85] F.G. Avci, B.S. Akbulut, E. Ozkirimli, Membrane active peptides and their biophysical characterization, Biomolecules 8 (2018), https://doi.org/10.3390/biom8030077.

[86] W.E. Robinson Jr., B. McDougall, D. Tran, M.E. Selsted, Anti-HIV-1 activity of indolicidin, an antimicrobial peptide from neutrophils, J. Leukoc. Biol. 63 (1998) 94–100.

[87] B. Yasin, M. Pang, J.S. Turner, Y. Cho, N.N. Dinh, A.J. Waring, R.I. Lehrer, E. A. Wagar, Evaluation of the inactivation of infectious herpes simplex virus by host-defense peptides, Eur. J. Clin. Microbiol. Infect. Dis. 19 (2000) 187–194.

[88] I. Ahmad, W.R. Perkins, D.M. Lupan, M.E. Selsted, A.S. Janoff, Liposomal entrapment of the neutrophil-derived peptide indolicidin endows it with in vivo antifungal activity, Biochim. Biophys. Acta 1237 (1995) 109–114.

[89] S.B. Aley, M. Zimmerman, M. Hetsko, M.E. Selsted, F.D. Gillin, Killing of Giardia lamblia by cryptdins and cationic neutrophil peptides, Infect. Immun. 62 (1994) 5397–5403.

[90] D.V. Laurents, Polyglutamine binding peptide 1 (QBP1) (2014), https://doi.org/10.13018/BMR25022.

[91] J.H. Davis, The description of membrane lipid conformation, order and dynamics by 2H-NMR, Biochim. Biophys. Acta 737 (1983) 117–171.

[92] J.E. Rothman, J. Lenard, Membrane asymmetry, Science 195 (1977) 743–753.

[93] J.P. Slotte, B. Ramstedt, The functional role of sphingomyelin in cell membranes, Eur. J. Lipid Sci. Technol. 109 (2007) 977–981.

[94] M. Hachem, A.H. Ali, I. Yildiz, C. Landry, F. Gosselet, Investigation of Lysophospholipids-DHA transport across an human model of blood brain barrier, Heliyon 10 (2024) e38871.

[95] L. Gaume, H. Chabrolles, M. Bisseux, I. Lopez-Coqueiro, L. Dehouck, A. Mirand, C. Henquell, F. Gosselet, C. Archimbaud, J.-L. Bailly, Enterovirus A71 crosses a human blood-brain barrier model through infected immune cells, Microbiol. Spectr. 12 (2024) e0069024.

[96] C. Menaceur, O. Dusailly, F. Gosselet, L. Fenart, J. Saint-Pol, Vesicular trafficking, a mechanism controlled by Cascade activation of Rab proteins: focus on Rab27, Biology (Basel) 12 (2023), https://doi.org/10.3390/biology12121530.

[97] S. Shelly, S. Liraz Zaltsman, O. Ben-Gal, A. Dayan, I. Ganmore, C. Shemesh, D. Atrakchi, S. Garra, O. Ravid, D. Rand, H. Israelov, T. Alon, G. Lichtenstein, S. Sharabi, D. Last, F. Gosselet, V. Rosen, G. Burstein, A. Friedlander, R. Harel, G. Vogel, M. Schnaider Beeri, Y. Mardor, Y. Lampl, G. Fleminger, I. Cooper, Potential neurotoxicity of titanium implants: prospective, in-vivo and in-vitro study, Biomaterials 276 (2021) 121039.

[98] F. Ramos-Martín, N. D'Amelio, Biomembrane lipids: when physics and chemistry join to shape biological activity, Biochimie 203 (2022) 118–138.

[99] C. Galanth, F. Abbassi, O. Lequin, J. Ayala-Sanmartin, A. Ladram, P. Nicolas, M. Amiche, Mechanism of antibacterial action of dermaseptin B2: interplay between helix-hinge-helix structure and membrane curvature strain, Biochemistry 48 (2009) 313–327.

[100] A. Tari, L. Huang, Structure and function relationship of phosphatidylglycerol in the stabilization of the phosphatidylethanolamine bilayer, Biochemistry 28 (1989) 7708–7712.

[101] G. Shahane, W. Ding, M. Palaiokostas, H.S. Azevedo, M. Orsi, Interaction of antimicrobial Lipopeptides with bacterial lipid bilayers, J. Membr. Biol. 252 (2019) 317–329.

[102] E. Wang, H. Sun, J. Wang, Z. Wang, H. Liu, J.Z.H. Zhang, T. Hou, End-point binding free energy calculation with MM/PBSA and MM/GBSA: strategies and applications in drug design, Chem. Rev. 119 (2019) 9478–9508.

[103] E.S. Salnikov, A.J. Mason, B. Bechinger, Membrane order perturbation in the presence of antimicrobial peptides by (2)H solid-state NMR spectroscopy, Biochimie 91 (2009) 734–743.

[104] M.H. Ali, B. Moghaddam, D.J. Kirby, A.R. Mohammed, Y. Perrie, The role of lipid geometry in designing liposomes for the solubilisation of poorly water soluble drugs, Int. J. Pharm. 453 (2013) 225–232.

[105] I. Wiegand, K. Hilpert, R.E.W. Hancock, Agar and broth dilution methods to determine the minimal inhibitory concentration (MIC) of antimicrobial substances, Nat. Protoc. 3 (2008) 163–175.

[106] S. Sánchez-Gómez, M. Lamata, J. Leiva, S.E. Blondelle, R. Jerala, J. Andrä, K. Brandenburg, K. Lohner, I. Moriyón, G. Martínez-de-Tejada, Comparative analysis of selected methods for the assessment of antimicrobial and membrane-permeabilizing activity: a case study for lactoferricin derived peptides, BMC Microbiol. 8 (2008) 196.

[107] G. Manzo, P.M. Ferguson, V.B. Gustilo, C.K. Hind, M. Clifford, T.T. Bui, A. F. Drake, R.A. Atkinson, J.M. Sutton, G. Batoni, C.D. Lorenz, D.A. Phoenix, A. J. Mason, Minor sequence modifications in temporin B cause drastic changes in antibacterial potency and selectivity by fundamentally altering membrane activity, Sci. Rep. 9 (2019) 1385.

[108] J. Gutierrez, A. Bakke, M. Vatta, A.R. Merrill, Plant natural products as antimicrobials for control of: a causative agent of the common scab disease, Front. Microbiol. 12 (2021) 833233.

[109] S.S. Bobde, F.M. Alsaab, G. Wang, M.L. Van Hoek, Ab initio designed antimicrobial peptides against gram-negative Bacteria, Front. Microbiol. 12 (2021), https://doi.org/10.3389/fmicb.2021.715246.

[110] W.L. Cheung-Lee, M.E. Parry, A. Jaramillo Cartagena, S.A. Darst, A.J. Link, Discovery and structure of the antimicrobial lasso peptide citrocin, J. Biol. Chem. 294 (2019) 6822–6830.

[111] N. Silber, C.L. Matos de Opitz, C. Mayer, P. Sass, Cell division protein FtsZ: from structure and mechanism to antibiotic target, Future Microbiol. 15 (2020) 801–831.

[112] C.N. Tagousop, J.-D. Tamokou, I.C. Kengne, D. Ngnokam, L. Voutquenne-Nazabadioko, Antimicrobial activities of saponins from Melanthera elliptica and their synergistic effects with antibiotics against pathogenic phenotypes, Chem. Cent. J. 12 (2018) 97.

[113] J.D.D. Tamokou, A.T. Mbaveng, V. Kuete, Antimicrobial activities of African medicinal spices and vegetables, Medicinal Spices and Vegetables from Africa (2017) 207–237, https://doi.org/10.1016/b978-0-12-809286-6.00008-x.

[114] M. Aschi, N. Perini, N. Bouchemal, C. Luzi, P. Savarin, L. Migliore, A. Bozzi, M. Sette, Structural characterization and biological activity of Crabrolin peptide isoforms with different positive charge, Biochim. Biophys. Acta Biomembr. 1862 (2020) 183055.

[115] F. Ramos-Martín, N. D'Amelio, Drug resistance: an incessant fight against evolutionary strategies of survival, Microbiol. Res. 14 (2023) 507–542.
[116] A. Singh, T. Prasad, K. Kapoor, A. Mandal, M. Roth, R. Welti, R. Prasad, Phospholipidome of Candida: each species of Candida has distinctive phospholipid molecular species, OMICS 14 (2010) 665–677.
[117] X. Feng, S. Jin, M. Wang, Q. Pang, C. Liu, R. Liu, Y. Wang, H. Yang, F. Liu, Y. Liu, The critical role of tryptophan in the antimicrobial activity and cell toxicity of the duck antimicrobial peptide DCATH, Front. Microbiol. 11 (2020) 1146.
[118] J.C. Bozelli Jr., J. Yune, X. Dang, J.L. Narayana, G. Wang, R.M. Epand, Membrane activity of two short Trp-rich amphipathic peptides, Biochim. Biophys. Acta Biomembr. 1862 (2020) 183280.
[119] D. Kalafatovic, E. Giralt, Cell-penetrating peptides: design strategies beyond primary structure and Amphipathicity, Molecules 22 (2017), https://doi.org/10.3390/molecules22111929.
[120] H.A. Rydberg, M. Matson, H.L. Amand, E.K. Esbjörner, B. Nordén, Effects of tryptophan content and backbone spacing on the uptake efficiency of cell-penetrating peptides, Biochemistry 51 (2012) 5531–5539.
[121] Ü. Langel, Cell-translocation mechanisms of CPPs, CPP, Cell-Penetrating Peptides (2019) 359–394, https://doi.org/10.1007/978-981-13-8747-0_10.
[122] M. Seleem, S. Thangamani, M. Nepal, J. Chmielewski, Antibacterial activity and therapeutic efficacy of Fl-PRPRPL-5, a cationic amphiphilic polyproline helix, in a mouse model of staphylococcal skin infection, Drug Des. Devel. Ther. (2015) 5749, https://doi.org/10.2147/dddt.s94505.
[123] J. Kuriakose, V. Hernandez-Gordillo, M. Nepal, A. Brezden, V. Pozzi, M. N. Seleem, J. Chmielewski, Targeting intracellular pathogenic bacteria with unnatural proline-rich peptides: coupling antibacterial activity with macrophage penetration, Angew. Chem. Int. Ed. Engl. 52 (2013) 9664–9667.
[124] J. Wang, X. Dou, J. Song, Y. Lyu, X. Zhu, L. Xu, W. Li, A. Shan, Antimicrobial peptides: promising alternatives in the post feeding antibiotic era, Med. Res. Rev. 39 (2019) 831–859.
[125] E.L. Wu, X. Cheng, S. Jo, H. Rui, K.C. Song, E.M. Dávila-Contreras, Y. Qi, J. Lee, V. Monje-Galvan, R.M. Venable, J.B. Klauda, W. Im, CHARMM-GUI membrane builder toward realistic biological membrane simulations, J. Comput. Chem. 35 (2014) 1997–2004.
[126] M.J. Abraham, T. Murtola, R. Schulz, S. Páll, J.C. Smith, B. Hess, E. Lindahl, GROMACS: high performance molecular simulations through multi-level parallelism from laptops to supercomputers, SoftwareX 1-2 (2015) 19–25, https://doi.org/10.1016/j.softx.2015.06.001.
[127] J. Huang, S. Rauscher, G. Nawrocki, T. Ran, M. Feig, B.L. de Groot, H. Grubmüller, A.D. MacKerell, CHARMM36m: an improved force field for folded and intrinsically disordered proteins, Nat. Methods 14 (2016) 71–73.
[128] H.J.C. Berendsen, J.P.M. Postma, W.F. van Gunsteren, J. Hermans, Interaction models for water in relation to protein hydration, The Jerusalem Symposia on Quantum Chemistry and Biochemistry (1981) 331–342, https://doi.org/10.1007/978-94-015-7658-1_21.
[129] H.J.C. Berendsen, J.P.M. Postma, W.F. van Gunsteren, A. DiNola, J.R. Haak, Molecular dynamics with coupling to an external bath, J. Chem. Phys. 81 (1984) 3684–3690, https://doi.org/10.1063/1.448118.
[130] M. Parrinello, A. Rahman, Polymorphic transitions in single crystals: a new molecular dynamics method, J. Appl. Phys. 52 (1981) 7182–7190, https://doi.org/10.1063/1.328693.
[131] S. Nosé, M.L. Klein, Constant pressure molecular dynamics for molecular systems, Mol. Phys. 50 (1983) 1055–1076, https://doi.org/10.1080/00268978300102851.
[132] S. Nosé, A unified formulation of the constant temperature molecular dynamics methods, J. Chem. Phys. 81 (1984) 511–519, https://doi.org/10.1063/1.447334.
[133] W.G. Hoover, Canonical dynamics: equilibrium phase-space distributions, Phys. Rev. A Gen. Phys. 31 (1985) 1695–1697.
[134] U. Essmann, L. Perera, M.L. Berkowitz, T. Darden, H. Lee, L.G. Pedersen, A smooth particle mesh Ewald method, J. Chem. Phys. 103 (1995) 8577–8593, https://doi.org/10.1063/1.470117.
[135] S. Jo, T. Kim, W. Im, Automated builder and database of protein/membrane complexes for molecular dynamics simulations, PLoS One 2 (2007) e880.
[136] Ramos-Martín, F., Herrera-León, C., Antonietti, V., Sonnet, P., Sarazin, C., D'Amelio, N. Antimicrobial peptide K11 selectively recognizes bacterial biomimetic membranes and acts by twisting their bilayers, Pharmaceuticals 14 (2020). https://doi.org/10.3390/ph14010001.
[137] S. Buchoux, FATSLiM: a fast and robust software to analyze MD simulations of membranes, Bioinformatics 33 (2017) 133–134.
[138] M.S. Valdés-Tresanco, M.E. Valdés-Tresanco, P.A. Valiente, E. Moreno, gmx_MMPBSA: a new tool to perform end-state free energy calculations with GROMACS, J. Chem. Theory Comput. 17 (2021) 6281–6291.
[139] R. Koradi, M. Billeter, K. Wüthrich, MOLMOL: a program for display and analysis of macromolecular structures, J. Mol. Graph. 14 (1996) 51–55, 29-32.
[140] W. Humphrey, A. Dalke, K. Schulten, VMD: Visual molecular dynamics, J. Mol. Graph. 14 (1996) 33–38, https://doi.org/10.1016/0263-7855(96)00018-5.
[141] T. Williams, C. Kelley, E.A. Merritt, C. Bersch, H.B. Bröker, J. Campbell, R. Cunningham, D. Denholm, E. Elber, R. Fearick, Gnuplot 5.4. 4: an interactive plotting program. http://www.gnuplot.info/docs_5.4/Gnuplot_5_4.pdf, 2022.
[142] W.L.A.O. DeLano, Pymol: an open-source molecular graphics tool, CCP4 Newslett. Protein Crystallogr. 40 (2002) 82–92.
[143] A. Onufriev, D. Bashford, D.A. Case, Exploring protein native states and large-scale conformational changes with a modified generalized born model, Proteins 55 (2004), https://doi.org/10.1002/prot.20033.
[144] D.A. Case, H. Metin Aktulga, K. Belfon, I. Ben-Shalom, S.R. Brozell, D.S. Cerutti, T. E. Cheatham III, V.W.D. Cruzeiro, T.A. Darden, R.E. Duke, G. Giambasu, M. K. Gilson, H. Gohlke, A.W. Goetz, R. Harris, S. Izadi, S.A. Izmailov, C. Jin, K. Kasavajhala, M.C. Kaymak, E. King, A. Kovalenko, T. Kurtzman, T. Lee, S. LeGrand, P. Li, C. Lin, J. Liu, T. Luchko, R. Luo, M. Machado, V. Man, M. Manathunga, K.M. Merz, Y. Miao, O. Mikhailovskii, G. Monard, H. Nguyen, K. A. O'Hearn, A. Onufriev, F. Pan, S. Pantano, R. Qi, A. Rahnamoun, D.R. Roe, A. Roitberg, C. Sagui, S. Schott-Verdugo, J. Shen, C.L. Simmerling, N. R. Skrynnikov, J. Smith, J. Swails, R.C. Walker, J. Wang, H. Wei, R.M. Wolf, X. Wu, Y. Xue, D.M. York, S. Zhao, P.A. Kollman, Amber 2021, University of California, San Francisco, 2021.
[145] F. Shimizu, Y. Sano, M.-A. Abe, T. Maeda, S. Ohtsuki, T. Terasaki, T. Kanda, Peripheral nerve pericytes modify the blood-nerve barrier function and tight junctional molecules through the secretion of various soluble factors, J. Cell. Physiol. 226 (2011) 255–266.
[146] R. Cecchelli, S. Aday, E. Sevin, C. Almeida, M. Culot, L. Dehouck, C. Coisne, B. Engelhardt, M.-P. Dehouck, L. Ferreira, A stable and reproducible human blood-brain barrier model derived from hematopoietic stem cells, PLoS One 9 (2014) e99733.
[147] C. Deligne, J. Hachani, S. Duban-Deweer, S. Meignan, P. Leblond, A. M. Carcaboso, Y. Sano, F. Shimizu, T. Kanda, F. Gosselet, M.-P. Dehouck, C. Mysiorek, Development of a human in vitro blood-brain tumor barrier model of diffuse intrinsic pontine glioma to better understand the chemoresistance, Fluids Barriers CNS 17 (2020) 37.
[148] E.L.J. Moya, E. Vandenhaute, E. Rizzi, M.-C. Boucau, J. Hachani, N. Maubon, F. Gosselet, M.-P. Dehouck, Miniaturization and automation of a human in vitro blood-brain barrier model for the high-throughput screening of compounds in the early stage of drug discovery, Pharmaceutics 13 (2021), https://doi.org/10.3390/pharmaceutics13060892.
[149] D. Rand, O. Ravid, D. Atrakchi, H. Israelov, Y. Bresler, C. Shemesh, L. Omesi, S. Liraz-Zaltsman, F. Gosselet, T.S. Maskrey, M.S. Beeri, P. Wipf, I. Cooper, Endothelial iron homeostasis regulates blood-brain barrier integrity via the HIF2α-Ve-cadherin pathway, Pharmaceutics 13 (3) (2021) 311, https://doi.org/10.3390/pharmaceutics13030311.
[150] A. Paul, A. Huber, D. Rand, F. Gosselet, I. Cooper, E. Gazit, D. Segal, Naphthoquinone-dopamine hybrids inhibit α-Synuclein aggregation, disrupt preformed fibrils, and attenuate aggregate-induced toxicity, Chemistry 26 (2020) 16486–16496.
[151] A.-G. Calas, A.-S. Hanak, N. Jaffré, A. Nervo, J. Dias, C. Rousseau, C. Courageux, X. Brazzolotto, P. Villa, A. Obrecht, J.-F. Goossens, C. Landry, J. Hachani, F. Gosselet, M.-P. Dehouck, J. Yerri, M. Kliachyna, R. Baati, F. Nachon, Efficacy assessment of an uncharged reactivator of NOP-inhibited acetylcholinesterase based on Tetrahydroacridine pyridine-Aldoxime hybrid in mouse compared to Pralidoxime, Biomolecules 10 (2020), https://doi.org/10.3390/biom10060858.
[152] M.-P. Dehouck, M. Tachikawa, Y. Hoshi, K. Omori, C.-A. Maurage, G. Strecker, L. Dehouck, M.-C. Boucau, Y. Uchida, F. Gosselet, T. Terasaki, Y. Karamanos, Quantitative targeted absolute proteomics for better characterization of an in vitro human blood-brain barrier model derived from hematopoietic stem cells, Cells 11 (2022), https://doi.org/10.3390/cells11243963.
[153] R. Cecchelli, B. Dehouck, L. Descamps, L. Fenart, V. Buée-Scherrer, C. Duhem, S. Lundquist, M. Rentfel, G. Torpier, M.P. Dehouck, In vitro model for evaluating drug transport across the blood-brain barrier, Adv. Drug Deliv. Rev. 36 (1999) 165–178.
[154] F. Ramos-Martín, C. Herrera-León, V. Antonietti, P. Sonnet, C. Sarazin, N. D'Amelio, The potential of antifungal peptide Sesquin as natural food preservative, Biochimie 203 (2022) 51–64.
[155] J.H. Davis, K.R. Jeffrey, M. Bloom, M.I. Valic, T.P. Higgs, Quadrupolar echo deuteron magnetic resonance spectroscopy in ordered hydrocarbon chains, Chem. Phys. Lett. 42 (1976) 390–394, https://doi.org/10.1016/0009-2614(76)80392-2.
[156] R.M. Humphries, J. Ambler, S.L. Mitchell, M. Castanheira, T. Dingle, J.A. Hindler, L. Koeth, K. Sei, CLSI methods development and standardization working Group of the Subcommittee on antimicrobial susceptibility testing, CLSI methods development and standardization working group. Best practices for evaluation of antimicrobial susceptibility tests, J. Clin. Microbiol. 56 (2018), https://doi.org/10.1128/JCM.01934-17.